

STABLE HYBRID UPWINDING VAG SCHEME FOR THE INCOMPRESSIBLE DIPHASIC MODEL WITH DISCONTINUOUS CAPILLARY PRESSURE

THOMAS CROZON¹, ROLAND MASSON², EL HOUSSAINE QUENJEL^{3,*} AND MAZEN SAAD⁴

Abstract. In this work, we propose an improved discretization, in terms of stability and accuracy, for the incompressible two-phase Darcy flows in a heterogeneous porous medium with discontinuous capillary forces. For this purpose, the total velocity formulation of the model is used. The coupled system is composed of a degenerate parabolic equation for the non-wetting phase and a pressure equation for the total velocity. We combine a positive Vertex Approximation Gradient (VAG) type scheme for the gradient fluxes with a hybrid upwinding of the mobilities. This approach entails a maximum principle on the saturations, which remain in their physical ranges. Energy estimates are obtained by selecting key approximations of the fluxes. These stability results allow to prove the existence of discrete solutions. Numerical experiments on complex test-cases show the robustness of the new approach in terms of the accuracy as well as the nonlinear convergence. Comparison to the usual phase potential upwinding approach and to a previous hybrid upwinding scheme are also provided.

Mathematics Subject Classification. 35K55, 35K65, 65M08, 65M12.

Received June 25, 2025. Accepted February 8, 2026.

1. INTRODUCTION

The diphasic system in porous media is a model of reference in subsurface flow engineering [4, 7, 22, 38]. It arises in technologies simulating the CO₂ sequestration, the Hydrogen storage or enhanced oil recovery. It is also used in modeling and processing high-energy geothermal systems.

The inherent heterogeneity of natural porous media gives rise to discontinuous spatial variations in physical properties, posing challenges for the modeling and discretization of two-phase Darcy flows. This work focuses on the numerical challenges raised by heterogeneous rock-type properties such as permeability and capillary pressure laws, leading potentially to highly contrasted velocities and highly nonlinear transmission conditions at the interfaces between different rock-types. This is typically the case of flow in fractured porous media which has been the object of intensive research during the last two decades [13, 37, 41]. Capturing all of these elements is a challenging task. Several solvers have been already proposed on the subject in the literature based

Keywords and phrases. Degenerate compressible two-phase Darcy flow, hybrid-upwinding, VAG scheme.

¹ Université de Lille, Inria CNRS, UMR 8524 – Laboratoire Paul Painlevé, F-59000 Lille, France.

² Université Côte d’Azur, Inria, CNRS, Laboratoire J.A. Dieudonné, Team Galets, Nice, France.

³ Laboratoire MIA, Bâtiment Pascal, Pôle Sciences et Technologie, La Rochelle Université, 23 Avenue A. Einstein, 17031 La Rochelle Cedex, France.

⁴ Ecole Centrale de Nantes, LMJL, CNRS UMR 6629, 1 rue de la Noë, 44321 Nantes, France.

*Corresponding author: el-houssaine.quenjel@univ-lr.fr

on Finite Volume discretizations [13, 14, 19, 24, 34], Gradient schemes [31], high order Discontinuous Galerkin discretizations [6, 27] possibly combined with a Mixed Finite Element method as in [35], and space-time domain decomposition methods as in [1] for a purely capillary diffusive two-phase flow model. However, convergent, robust and efficient numerical scheme taking into account the model degeneracy and heterogeneous rock-types in 3D on general meshes is still under active research.

In this paper, we focus on the development of a new scheme for the diphasic problem with discontinuous capillary pressure laws that is based on the Vertex Approximate Gradient (VAG) discretization [13, 14, 31]. Making use of vertices and cell centers as the main degrees of freedom, the VAG discretization is dotted with several advantages. First, the distribution of the cell porous volumes on the vertices is achieved in order to avoid mixture of different rock-types in the same control volume as opposed to classical Control Volume Finite Element (CVFE) methods. Second, it captures the discontinuity of the saturations at heterogeneous rock-type interfaces as far as the heterogeneities are conforming with respect to the mesh. Third, the discrete problem size can be reduced by eliminating the cell unknowns at the linear solver stage without any fill-in. The nonlinear convergence of the VAG solver can be enhanced using a switching of variable technique based on capillary pressure graphs parametrization [14]. It plays a crucial role to account for general capillary pressures curves exhibiting low regularity or asymptotics. The VAG scheme integrates efficiently with the state-of-the-art of CPR-AMG preconditioner and delivers particularly high CPU-time efficiency on simplicial meshes thanks to its essentially nodal structure. It has been extensively used on realistic test cases in particular for geothermal simulations [3]. On the other hand cell center approaches like TPFA or MPFA and Mixed Hybrid Methods are better adapted to hexahedral meshes. Discontinuous Galerkin methods provide accurate solutions, but are usually considered to be quite expensive for applications on realistic reservoir simulations compared with low order approaches.

Hybrid Upwinding (HU) schemes [32–34] have been designed as a more robust alternative to the Phase Potential Upwinding (PPU) approach [10, 25]. As a result of counter-flow fluxes, the latter suffers from the presence of kinks in the fluxes, which may raise some difficulties to the nonlinear convergence. Thanks to its total velocity formulation combined with an upwind approximation of the total velocity, capillary and gravity terms, the better smoothness properties of the HU fluxes improves the solver nonlinear convergence for long-term simulations of flows in heterogeneous media. In [16], the authors were able to extend the HU idea to the framework of the VAG scheme. The positivity of the solution is ensured by incorporating the techniques of Quenjel [39] in the diffusive capillary term. On the other hand, stability results such as energy estimates could not be obtained because of the Multi-Point nature of the VAG fluxes discretization. Using the physical primary variables, the first work addressing the convergence of a finite volume scheme with Two-Point Flux Approximation (TPFA) for the degenerate diphasic model with discontinuous capillary pressure was proposed in [17].

In this work, we propose an improved variant of the Hybrid Upwinding VAG (HU-VAG) scheme for the incompressible two-phase flow in porous media with different rock-types. A proper approximation of the generalized fluxes is proposed to reinforce the stability properties of the scheme. The key idea is to set up a direct link between the discrete total velocity and the discrete global pressure. For this purpose, the expression of the fractional flows in the pressure equation is computed implicitly through a nonlinear formula at each interface. This modification offers a couple of important mathematical properties that could not be established using the scheme of [16] while preserving the maximum principle property. More importantly, it allows the derivation of essential energy estimates on both the global pressure and a capillary energy term. As a consequence, one can make use of these ingredients to prove the existence result of the fully coupled nonlinear algebraic system derived from the numerical scheme. Up to our knowledge, this original contribution is new in the context of Multi-Point discretizations for degenerate models of incompressible immiscible two-phase flows in heterogeneous media.

Several typical test cases are conducted to shed light on the assets of the new HU numerical scheme. In addition to theoretical stability features, it offers a reduced numerical diffusion compared to our previous HU solver [16]. This is due to key approximations of the fluxes and the mobilities. They exhibit quasi-similar behavior

in terms of the nonlinear convergence and performance while requiring much fewer iterations than the PPU solver.

The remaining of this article is structured as follows. In Sections 2.1 and 2.2, the heterogeneous incompressible two-phase Darcy flow model is described, with its total velocity formulation as well as the main assumptions on the data. In Section 3, we present the VAG discretization with the polytopal mesh described in Section 3.1 and the definition of VAG Darcy fluxes and porous volumes in Section 3.2. The definitions of the primary and secondary unknowns of the two-phase flow model with the capillary pressure graph parametrization, the discrete global pressure and the mobility weighted capillary pressure are introduced in Section 3.3. The HU-VAG scheme of the two-phase flow model is then defined in Section 3.4. In Section 4, the mathematical properties satisfied by the new numerical scheme are established; namely, the physical bounds on the saturations together with the energy estimates on the global pressure and on the mobility weighted capillary pressure. The existence result is then stated where the proof follows the pathway proposed in [23]. Numerical experiments are carried out in Section 5. The paper is concluded in Section 6.

2. MODEL

2.1. The two-phase Darcy flow problem

We consider a polyhedral bounded domain Ω of \mathbb{R}^d ($3 \geq d \geq 1$) partitioned into a set of rock-type polyhedral subdomains denoted by $(\Omega_{rt})_{rt \in \mathcal{RT}}$ where \mathcal{RT} is the set of rock-types. Denoting $(0, t_f)$ (with $t_f < +\infty$) the time interval, we denote by $Q_{t_f} = \Omega \times (0, t_f)$ the space time domain. The porous medium is considered heterogeneous when its petrophysical properties vary with the rock-type. We denote the wetting phase by w and the non-wetting phase by nw . We consider immiscible and incompressible two-phase Darcy flow, which is governed by the following equations (see [7, 22])

$$\begin{cases} \phi(x)\partial_t s^\alpha + \operatorname{div} V^\alpha = 0, & \alpha \in \{nw, w\}, \\ \mathbf{V}^\alpha = -M^\alpha(x, s^\alpha)\Lambda(x)\nabla p^\alpha \\ p_c = p^{nw} - p^w \in \tilde{P}_c(x, s^{nw}), \\ s^{nw} + s^w = 1, \end{cases} \tag{2.1}$$

neglecting gravity for the sake of simplicity. In (2.1) $\phi(x)$ is the porosity of the medium, $\Lambda(x)$ its permeability tensor, s^α the α -phase saturation, p^α the phase pressure, \mathbf{V}^α the phase velocity that is given by the diphasic Darcy law, and p_c the capillary pressure. We denote by $M^\alpha(x, s^\alpha)$ the phase mobility, defined as the ratio between the relative permeability $k_r^\alpha(x, s^\alpha)$ to the phase dynamic viscosity μ^α . The function $\tilde{P}_c(x, s)$ represents the monotone graph extension of the capillary pressure function. The spatial dependence of \tilde{P}_c and M^α is assumed piecewise constant within each rock-type subdomain. This extension captures transmission conditions for the phases occurring at the interface between different rock-types. If a phase is present then its pressure must be continuous at the interface [43]. This permits well-observed oil-trapping effect [9, 18, 19, 26] that has been studied in [21] for 3D domains.

We complete the system (2.1) with initial data for the selected variables and impose appropriate boundary conditions

$$\mathbf{V}^\alpha \cdot \mathbf{n} = 0 \quad \text{on } \Gamma^N \times (0, t_f), \quad p^\alpha = p_{Dir}^\alpha \quad \text{on } \Gamma^{Dir} \times (0, t_f) \quad \text{for } \alpha \in \{nw, w\},$$

where \mathbf{n} is the outward unit normal vector to Γ^N . We assume that $\{\Gamma^{Dir}, \Gamma^N\}$ is a partition of $\partial\Omega$ such that $|\Gamma^{Dir}| > 0$. To introduce the total velocity formulation, let us first define the total mobility (see [22]) and total velocity as follows

$$\begin{aligned} M(x, s^{nw}) &= M^{nw}(x, s^{nw}) + M^w(x, s^w) \quad \text{for a.e. } x \in \Omega, \\ \mathbf{V}^T &= - \sum_{\alpha \in \{nw, w\}} M^\alpha(x, s^\alpha)\Lambda(x)\nabla p^\alpha. \end{aligned} \tag{2.2}$$

We also define the fractional flow functions

$$f^{\text{nw}}(x, s^{\text{nw}}) = \frac{M^{\text{nw}}(x, s^{\text{nw}})}{M(x, s^{\text{nw}})}, \quad f^{\text{w}}(x, s^{\text{w}}) = 1 - f^{\text{nw}}(x, s^{\text{nw}}) = \frac{M^{\text{w}}(x, s^{\text{w}})}{M(x, s^{\text{nw}})}.$$

This allows us to express the phase Darcy velocities with respect to the total velocity as follows

$$\begin{aligned} \mathbf{V}^{\text{nw}} &= \underbrace{f^{\text{nw}}(x, s^{\text{nw}})\mathbf{V}^T}_{\text{fractional flow term}} + \underbrace{\frac{M^{\text{nw}}(x, s^{\text{nw}})M^{\text{w}}(x, s^{\text{w}})}{M(x, s^{\text{nw}})}(-\Lambda(x)\nabla p_c)}_{\text{capillary diffusion term}}, \\ \mathbf{V}^{\text{w}} &= \underbrace{f^{\text{w}}(x, s)\mathbf{V}^T}_{\text{fractional flow term}} + \underbrace{\frac{M^{\text{nw}}(x, s^{\text{nw}})M^{\text{w}}(x, s^{\text{w}})}{M(x, s^{\text{nw}})}(\Lambda(x)\nabla p_c)}_{\text{capillary diffusion term}}, \end{aligned}$$

leading to the following total velocity formulation of (2.1)

$$\begin{cases} \phi(x)\partial_t s^{\text{nw}} + \operatorname{div}\left(f^{\text{nw}}(x, s)\mathbf{V}^T - \frac{M^{\text{nw}}(x, s^{\text{nw}})M^{\text{w}}(x, s^{\text{w}})}{M(x, s^{\text{nw}})}\Lambda(x)\nabla p_c\right) = 0, \\ \operatorname{div}\mathbf{V}^T = 0, \\ p_c = p^{\text{nw}} - p^{\text{w}} \in \tilde{P}_c(x, s^{\text{nw}}), \\ s^{\text{nw}} + s^{\text{w}} = 1. \end{cases} \quad (2.3)$$

2.2. Assumptions

Let us specify the main assumptions on the physical data and nonlinearities. They are classical in the study of diphasic flow in porous media.

- (A₀) The initial pressures $p_0^{\text{nw}}, p_0^{\text{w}}$ are $L^2(\Omega)$ -functions and the initial saturations of the α -phases are $L^\infty(\Omega)$ -functions such that $0 \leq s_0^\alpha(x) \leq 1$ for a.e. $x \in \Omega$.
- (A₁) The porosity ϕ is in $L^\infty(\Omega)$ and there exist $\underline{\phi}, \bar{\phi} > 0$ such that: $\underline{\phi} \leq \phi(x) \leq \bar{\phi}$ for a.e. x in Ω .
- (A₂) For each $\alpha \in \{\text{nw}, \text{w}\}$ the mobility function is space dependent and given by

$$M^\alpha(x, s) = \sum_{\text{rt} \in \mathcal{RT}} M_{\text{rt}}^\alpha(s) \mathbf{1}_{\Omega_{\text{rt}}}(x), \quad \text{for a.e. } x \in \Omega_{\text{rt}},$$

where $\mathbf{1}_{\Omega_{\text{rt}}}$ is the characteristic function of the subdomain Ω_{rt} . Each mobility M_{rt}^α is a non-decreasing continuous function on \mathbb{R} , such that: $M_{\text{rt}}^\alpha(s) = 0$ for all $s \leq 0$ and $M_{\text{rt}}^\alpha(s) = M_{\text{rt}}^\alpha(1)$ for all $s \geq 1$. Moreover, the total mobility (2.2) is bounded from below and above in the sense that there exists $M_{\max} \geq m_{\min} > 0$ such that:

$$m_{\min} \leq M(x, s) = M^{\text{nw}}(x, s) + M^{\text{w}}(x, 1 - s) \leq M_{\max} \quad \text{for a.e. } x \in \Omega, \quad \forall s \in \mathbb{R}.$$

- (A₃) The intrinsic permeability is a symmetric positive-definite matrix and is essentially bounded. It is also uniformly elliptic *i.e.* there exist constants $\underline{\Lambda}$ and $\bar{\Lambda}$ such that

$$\underline{\Lambda}|z|^2 \leq \Lambda(x)z \cdot z \leq \bar{\Lambda}|z|^2 \quad \text{for all } z \in \mathbb{R}^d \quad \text{and a.e. } x \in \Omega.$$

- (A₄) Each rock-type $\text{rt} \in \mathcal{RT}$ has its own capillary pressure function $P_{c,\text{rt}}(s^{\text{nw}})$. It is assumed to be non-decreasing and in $C^1([0, 1], \mathbb{R})$. We define its monotone graph extension as in [16, 21] by

$$\tilde{P}_{c,\text{rt}}(s) = \begin{cases} [-\infty, P_{c,\text{rt}}(0)] & \text{if } s = 0, \\ P_{c,\text{rt}}(s) & \text{if } s \in (0, 1), \\ [P_{c,\text{rt}}(1), +\infty] & \text{if } s = 1, \end{cases}$$

and we set

$$\tilde{P}_c(x, s) = \sum_{\text{rt} \in \mathcal{RT}} \tilde{P}_{c,\text{rt}}(s) \mathbf{1}_{\Omega_{\text{rt}}}(x), \quad \text{for a.e. } x \in \Omega_{\text{rt}}.$$

- **(A₅)** The inverse of the capillary pressure graph is defined in each rock type by $S_{\text{rt}}^{\text{nw}}$. It is a continuous nondecreasing function from $[0, 1]$ to $\overline{\mathbb{R}}$. Consider

$$\Pi_{\text{rt}}(v) = \int_0^v u S_{\text{rt}}^{\text{nw}}(u)' \, du,$$

where $u \rightarrow u S_{\text{rt}}^{\text{nw}}(u)'$ is assumed to be in $L^1(\mathbb{R}^+)$.

3. THE VAG DISCRETIZATION

The Vertex Approximation Gradient (VAG) method is a control volume method (as the Control Volume Finite Element method) in the sense that it solves a volume balance equation at each degree of freedom located at the cell centers and vertices.

3.1. Generalized polyhedral mesh

We consider a set \mathcal{M} of disjoint open polyhedral subsets of Ω such that $\cup_{k \in \mathcal{M}} \bar{k} = \bar{\Omega}$. Each cell $k \in \mathcal{M}$ is assumed to have a center $x_k \in k$, such that k is star-shaped with respect to x_k . We denote by $|k|$ the measure (volume) of the cell k . Each cell k has a set \mathcal{F}_k of faces, which are not required to be planar, thereby justifying the “generalized” nature of the mesh. Then, for a face σ , we denote by \mathcal{E}_σ its set of edges and by \mathcal{V}_σ its set of vertices. Accordingly, for a cell k , its set of vertices is given by $\mathcal{V}_k = \cup_{\sigma \in \mathcal{E}_k} \mathcal{V}_\sigma$. We define the set vertices of the mesh as $\mathcal{V} = \cup_{k \in \mathcal{M}} \mathcal{V}_k$, the set of faces as $\mathcal{F} = \cup_{k \in \mathcal{M}} \mathcal{F}_k$, and the set of edges as $\mathcal{E} = \cup_{\sigma \in \mathcal{F}} \mathcal{E}_\sigma$. For a vertex $s \in \mathcal{V}$, we denote by \mathcal{M}_s the subset of cells sharing the vertex s . Finally, we denote by l_k and l_s the number of vertices sharing a cell k , and the number of cells sharing a vertex s :

$$l_k = \#\mathcal{V}_k, \quad l_s = \#\mathcal{M}_s, \quad \forall k \in \mathcal{M}, \quad \forall s \in \mathcal{V}.$$

Let us define the parameter

$$l_{\mathcal{D}} = \max \left(\max_{\beta \in \mathcal{M} \cup \mathcal{V}} l_\beta, \max_{k \in \mathcal{M}} \#\mathcal{F}_k \right), \tag{3.1}$$

which quantifies the mesh regularity.

The VAG discretization introduced in [29] considers both vertices and cell centers as degrees of freedom, it is based on the following vector space of discrete unknowns

$$X_{\mathcal{D}} = \{v_k \in \mathbb{R}, \quad v_s \in \mathbb{R}, \quad k \in \mathcal{M}, \quad s \in \mathcal{V}\}.$$

We assume that for any $\sigma \in \mathcal{F}$, a so-called face center $x_\sigma \in \sigma \setminus \cup_{e \in \mathcal{E}_\sigma} e$ can be defined as a convex combination of its vertices:

$$x_\sigma = \sum_{s \in \mathcal{V}_\sigma} \beta_{\sigma,s} x_s, \quad \text{with} \quad \sum_{s \in \mathcal{V}_\sigma} \beta_{\sigma,s} = 1, \quad \text{and} \quad \beta_{\sigma,s} \geq 0 \quad \text{for all} \quad s \in \mathcal{V}_\sigma.$$

Then, the face σ is supposed to be given by the union of the triangles $T_{\sigma,e}$, defined by the face center x_σ and an edge $e \in \mathcal{E}_\sigma$. One can build \mathcal{T} , a tetrahedral sub-mesh of \mathcal{M} , given by $\mathcal{T} = \{T_{k,\sigma,e}, e \in \mathcal{E}_\sigma, \sigma \in \mathcal{F}, k \in \mathcal{M}\}$ where $T_{k,\sigma,e}$ is the tetrahedron joining the cell center x_k to the triangle $T_{\sigma,e}$. We measure the regularity and the mesh size of this simplicial mesh with the parameters

$$\theta_{\mathcal{T}} = \max_{T \in \mathcal{T}} \frac{h_T}{\rho_T}, \tag{3.2}$$

and

$$h_{\mathcal{T}} = \max_{T \in \mathcal{T}} h_T, \tag{3.3}$$

where h_T and ρ_T are respectively the diameter of T and its insphere diameter. A second order interpolation operator is defined at each face center x_σ , $\sigma \in \mathcal{F}$, such that for any $v_{\mathcal{D}} \in X_{\mathcal{D}}$

$$I_\sigma(v_{\mathcal{D}}) = \sum_{s \in \mathcal{V}_\sigma} \beta_{\sigma,s} v_s.$$

The mesh \mathcal{M} is supposed to be conforming with respect to the partition of Ω into the subdomains Ω_{rt} , and to the partition $\{\Gamma^{\text{Dir}}, \Gamma^N\}$ of $\partial\Omega$. It means that for every cell $k \in \mathcal{M}$ there exists a unique $\text{rt}_k \in \mathcal{RT}$ such that $k \subset \Omega_{\text{rt}_k}$. For the vertices, let us set $\chi_s = \{\text{rt}_k, k \in \mathcal{M}_s\} \subset \mathcal{RT}$ the subset of rock-types sharing the node $s \in \mathcal{V}$. Then, we define $\chi_k = \{\text{rt}_k\}$ for all $k \in \mathcal{M}$. Finally, we denote by \mathcal{V}_{Dir} the set of nodes located at the Dirichlet boundary $\bar{\Gamma}^{\text{Dir}}$.

3.2. VAG fluxes and porous volumes

Let $v_{\mathcal{D}}$ be in $X_{\mathcal{D}}$, the function $\pi_{\mathcal{T}} v_{\mathcal{D}} \in H^1(\Omega)$ is the continuous piecewise affine function on each tetrahedron of \mathcal{T} such that $\pi_{\mathcal{T}} v_{\mathcal{D}}(x_k) = v_k$, $\pi_{\mathcal{T}} v_{\mathcal{D}}(x_s) = v_s$ and $\pi_{\mathcal{T}} v_{\mathcal{D}}(x_\sigma) = I_\sigma(v_{\mathcal{D}})$ (see [28]). Then, we define the space $V_{\mathcal{T}} = \{\pi_{\mathcal{T}} u_{\mathcal{D}}, u_{\mathcal{D}} \in X_{\mathcal{D}}\} \subset H^1(\Omega)$. The nodal basis of this finite element discretization \mathcal{T} writes φ_k, φ_s for $k \in \mathcal{M}, s \in \mathcal{V}$ (the nodes of \mathcal{T} are the vertices and cell centers of \mathcal{M}).

In [29] the VAG fluxes $F_{k,s}(u_{\mathcal{D}})$, associated with $u_{\mathcal{D}} \in X_{\mathcal{D}}$, are derived from the finite element formulation of the problem, it connects the cell k to its vertex s . Therefore, the generalized VAG fluxes definition is given by the expression:

$$F_{k,s}(u_{\mathcal{D}}) = \int_k -\Lambda(x) \nabla \pi_{\mathcal{T}} u_{\mathcal{D}} \cdot \nabla \varphi_s \, dx = \sum_{s' \in \mathcal{V}_k} \mathbb{T}_k^{s,s'} (u_k - u'_s),$$

with

$$\mathbb{T}_k^{s,s'} = \int_k \Lambda(x) \nabla \varphi_{s'} \cdot \nabla \varphi_s \, dx.$$

For each cell $k \in \mathcal{M}$, let us define the symmetric positive definite matrix

$$A_k = \left(\mathbb{T}_k^{s,s'} \right)_{s,s' \in \mathcal{V}_k} \in \mathbb{R}^{l_k \times l_k}, \tag{3.4}$$

as in [20]. The linear operator $\delta_k : X_{\mathcal{D}} \rightarrow \mathbb{R}^{l_k}$ is defined for each $k \in \mathcal{M}$ by

$$(\delta_k v_{\mathcal{D}})_s = v_k - v_s, \quad \forall s \in \mathcal{V}_k, \quad \forall v_{\mathcal{D}} \in X_{\mathcal{D}}. \tag{3.5}$$

Then, one obtains

$$\int_k \Lambda(x) \nabla \pi_{\mathcal{T}} u_{\mathcal{D}} \cdot \nabla \pi_{\mathcal{T}} v_{\mathcal{D}} \, dx = \delta_k v_{\mathcal{D}} \cdot A_k \delta_k u_{\mathcal{D}}, \quad \forall u_{\mathcal{D}}, v_{\mathcal{D}} \in X_{\mathcal{D}}, \quad \forall k \in \mathcal{M}. \tag{3.6}$$

Let us now define the porous volumes assigned to each degree of freedom. They are obtained by distribution of the given cell porous volumes to its nodes taking into account the heterogeneity of the porous medium. Following [13, 30], setting

$$a_{k,s} = \frac{\mathbb{T}_k^s}{\sum_{k' \in \mathcal{M}_s} \mathbb{T}_{k'}^s} \quad \text{where} \quad \mathbb{T}_k^s = \sum_{s' \in \mathcal{V}_k \setminus \mathcal{V}_{\text{Dir}}} \mathbb{T}_k^{s,s'}.$$

For all $s \in \mathcal{V}_k \setminus \mathcal{V}_{\text{Dir}}$ and given $\omega > 0$, we set

$$\phi_{k,s} = \omega a_{k,s} \int_k \phi(x) \, dx,$$

and define the porous volumes for all $k \in \mathcal{M}$ and $s \in \mathcal{V} \setminus \mathcal{V}_{Dir}$ as

$$\begin{aligned} \phi_s &= \sum_{k \in \mathcal{M}_s} \phi_{k,s} = \omega \sum_{k \in \mathcal{M}_s} a_{k,s} \int_k \phi(x) \, dx, \\ \phi_k &= \int_k \phi(x) \, dx - \sum_{s \in \mathcal{V}_k \setminus \mathcal{V}_{Dir}} \phi_{k,s} = \int_k \phi(x) \, dx - \sum_{s \in \mathcal{V}_k \setminus \mathcal{V}_{Dir}} a_{k,s} \int_k \phi(x) \, dx \\ &= \left(1 - \omega \sum_{s \in \mathcal{V}_k \setminus \mathcal{V}_{Dir}} a_{k,s} \right) \int_k \phi(x) \, dx. \end{aligned}$$

The parameter ω is chosen small enough to guarantee the positivity of ϕ_k . This construction of the porous volumes avoids to enlarge artificially the drains at heterogeneous interfaces (see [13, 30]).

Let us now recall the following Lemma stating the VAG Darcy fluxes coercivity property which, plays a key role in the VAG scheme numerical analysis (see [11]).

Lemma 1 ([11], Lem. 3.1, coercivity of VAG fluxes). *The VAG Darcy fluxes satisfy the following coercivity property: for all $u_{\mathcal{D}} \in X_{\mathcal{D}}$ one has*

$$\sum_{s \in \mathcal{V}_k} (u_k - u_s) F_{k,s}(u_{\mathcal{D}}) = \int_k \Lambda(x) \nabla \pi_{\mathcal{T}} u_{\mathcal{D}} \cdot \nabla \pi_{\mathcal{T}} u_{\mathcal{D}} \, dx,$$

and

$$\underline{\Lambda} \|\nabla \pi_{\mathcal{T}} u_{\mathcal{D}}\|_{L^2(k)^d} \leq \sum_{s \in \mathcal{V}_k} (u_k - u_s) F_{k,s}(u_{\mathcal{D}}) \leq \bar{\Lambda} \|\nabla \pi_{\mathcal{T}} u_{\mathcal{D}}\|_{L^2(k)^d}.$$

3.3. Primary and secondary unknowns for the two-phase flow model

3.3.1. Capillary pressure graphs parametrization

The choice of the primary unknowns plays a key role in the convergence of the Newton method used to solve the implicit problem at each time step (see [5]). Here, the non-wetting phase pressure p^{nw} is classically chosen as the first primary unknown. The second primary unknown, denoted by τ must be chosen in such away to express the transmission conditions at heterogeneous rock-type interfaces and to enhance the stability of the Newton algorithm. Following [14, 16] our choice is based on a parametrization of the monotone graph extensions $\tilde{P}_{c,rt}$ of the capillary pressure functions. For each degree of freedom (d.o.f.) $\nu \in \mathcal{M} \cup \mathcal{V}$, we define non-decreasing continuous functions of τ

$$\begin{cases} P_{c,\chi_\nu}, \\ S_{\chi_\nu,rt}^{nw}, \text{ for all } rt \in \chi_\nu, \end{cases} \tag{3.7}$$

such that $P_{c,\chi_\nu}(\tau_\nu)$ is the capillary pressure at the d.o.f. ν and $S_{\chi_\nu,rt}^{nw}(\tau_\nu)$, $rt \in \chi_\nu$ are the non-wetting phase saturations at the d.o.f. ν (with as many values as rock-types around ν) capturing the saturation jumps for general capillary pressure functions. These functions are built such that for all $\tau \in [0, 1]$

$$\begin{cases} P_{c,\chi_\nu}(\tau) \in \tilde{P}_{c,rt}(S_{\chi_\nu,rt}^{nw}(\tau)), & \text{for all } rt \in \chi_\nu, \\ S_{\chi_\nu,rt}^{nw}(0) = 0, \quad S_{\chi_\nu,rt}^{nw}(1) = 1, & \text{for all } rt \in \chi_\nu, \\ P_{c,\chi_\nu}(0) = \min_{rt \in \chi_\nu} P_{c,rt}(0), \quad P_{c,\chi_\nu}(1) = \max_{rt \in \chi_\nu} P_{c,rt}(1), \\ P_{c,\chi_\nu}(\tau) + \sum_{rt \in \chi_\nu} S_{\chi_\nu,rt}^{nw}(\tau) & \text{is strictly increasing.} \end{cases}$$

For the analysis, we extend these functions outside of the interval $[0, 1]$ such that

$$\begin{cases} S_{\chi_\nu,rt}^{nw}(\tau) = \tau, & \text{if } \tau \in \mathbb{R} \setminus [0, 1], \\ P_{c,\chi_\nu}(\tau) = P_{c,\chi_\nu}(0) + \tau, & \text{if } \tau < 0, \\ P_{c,\chi_\nu}(\tau) = P_{c,\chi_\nu}(1) + \tau - 1, & \text{if } \tau > 1. \end{cases} \tag{3.8}$$

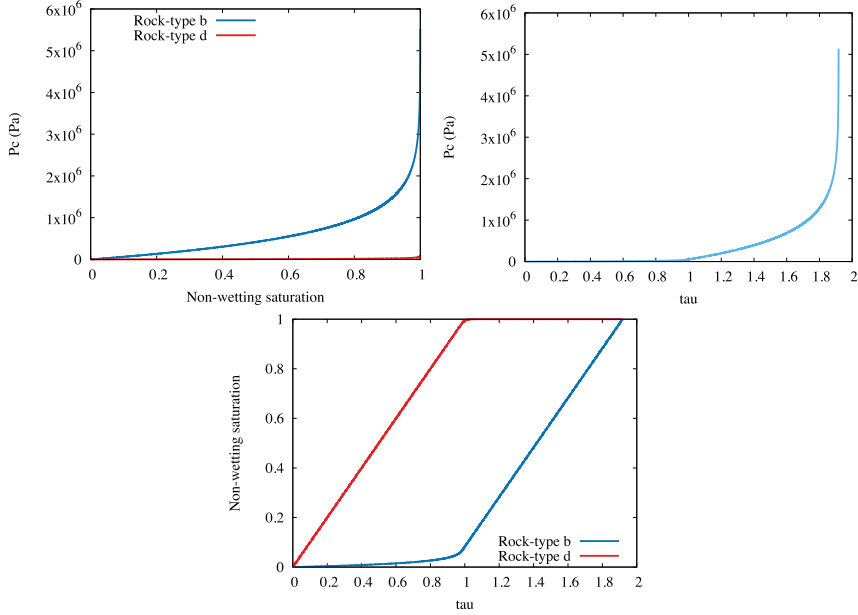


FIGURE 1. Example of capillary pressure functions obtained for $b_b = 10^4$ Pa and $b_d = 10^3$ Pa with the corresponding parametrizations of the capillary pressure $P_{c,\{b,d\}}(\tau)$ and of both rock-type saturations $S_{\{b,d\},d}^{\text{nw}}(\tau)$ and $S_{\{b,d\},b}^{\text{nw}}(\tau)$.

The non-wetting phase saturation as a function of τ is readily obtained by $S_{\chi_{\nu},\text{rt}}^{\text{w}}(\tau) = 1 - S_{\chi_{\nu},\text{rt}}^{\text{nw}}(\tau)$. One can refer to [14, 16] and to the numerical section (see Fig. 1) for examples of such parametrizations.

Then, the primary unknowns are defined by

$$p_{\mathcal{D}}^{\text{nw}} = (p_{\nu}^{\text{nw}})_{\nu \in \mathcal{M} \cup \mathcal{V}} \quad \text{and} \quad \tau_{\mathcal{D}} = (\tau_{\nu})_{\nu \in \mathcal{M} \cup \mathcal{V}}, \quad (3.9)$$

from which we derive the following secondary unknowns

$$\begin{cases} p_{c,\mathcal{D}} = (p_{c,\nu})_{\nu \in \mathcal{M} \cup \mathcal{V}}, & \text{with } p_{c,\nu} = P_{c,\chi_{\nu}}(\tau_{\nu}), \\ p_{\mathcal{D}}^{\text{w}} = (p_{\nu}^{\text{w}})_{\nu \in \mathcal{M} \cup \mathcal{V}}, & \text{where } p_{\nu}^{\text{w}} = p_{\nu}^{\text{nw}} - p_{c,\nu}, \\ s_k^{\alpha} = S_{\chi_k,\text{rt}_k}^{\alpha}(\tau_k), & k \in \mathcal{M}, \\ s_{k,s}^{\alpha} = S_{\chi_s,\text{rt}_k}^{\alpha}(\tau_s), & s \in \mathcal{V}, k \in \mathcal{M}_s. \end{cases}$$

Note that each phase pressure is uniquely defined at each degree of freedom while the saturations at a node s depend on the cell rock-type, therefore capturing the saturation jumps.

3.3.2. Global pressure and mobility weighted capillary pressure

Due to the degeneracy of the phase mobilities, energy estimates on the phase pressures cannot be obtained. To address this, a global pressure, interpreted as a weighted average of the phase pressures, is introduced in [2, 22]. Following the approach of Brenner *et al.* [12, 17], we adapt the artificial (or corrective) pressures to our VAG framework. In each rock-type $\text{rt} \in \mathcal{RT}$, we set

$$G_{\text{rt}_k}^{\text{nw}}(v) = \int_0^v f_{\text{rt}_k}^{\text{nw}}(S_{\text{rt}_k}^{\text{nw}}(u)) \, du, \quad G_{\text{rt}_k}^{\text{w}}(v) = \int_0^v f_{\text{rt}_k}^{\text{w}}(S_{\text{rt}_k}^{\text{w}}(u)) \, du,$$

leading to the following definition of the cell global pressure p_k , $k \in \mathcal{M}$ and to the node global pressures $p_{k,s}$, $s \in \mathcal{V}$, $k \in \mathcal{M}_s$, depending on the rock-type rt_k

$$\begin{cases} p_k = p_k^w + G_{rt_k}^{nw}(p_{c,k}) = p_k^{nw} - G_{rt_k}^w(p_{c,k}), & \text{for } k \in \mathcal{M}, \\ p_{k,s} = p_s^w + G_{rt_k}^{nw}(p_{c,s}) = p_s^{nw} - G_{rt_k}^w(p_{c,s}), & \text{for } s \in \mathcal{V}, k \in \mathcal{M}_s. \end{cases} \quad (3.10)$$

To address the control of the capillary diffusion term, let us also introduce for each rock-type $rt_k \in \mathcal{RT}$ the function ξ_{rt_k} , termed mobility weighted capillary pressure in the following, and defined by

$$\xi_{rt_k}(v) = \int_0^v \sqrt{M_{rt_k}^{nw}(S_{rt_k}^{nw}(u))} \sqrt{M_{rt_k}^w(1 - S_{rt_k}^{nw}(u))} du.$$

Then, the discrete mobility weighted capillary pressures are given by

$$\begin{cases} \xi_k = \xi_{rt_k}(p_{c,k}), & \text{for } k \in \mathcal{M}, \\ \xi_{k,s} = \xi_{rt_k}(p_{c,s}), & \text{for } s \in \mathcal{V}, k \in \mathcal{M}_s. \end{cases} \quad (3.11)$$

As the saturations, these mobility weighted capillary pressures are ‘‘discontinuous’’ at vertices sharing several rock-types, they encode the saturation jumps at the interface between rock-type subdomains.

3.4. The Hybrid Upwinding VAG discretization of the two-phase flow model

Following [16], to account for the potential discontinuity of the saturations at a given node s , let us define the functions

$$\begin{cases} \gamma_k^\alpha(\tau) = S_{\chi_k, rt_k}^\alpha(\tau), & k \in \mathcal{M}, \quad \alpha \in \{w, nw\}, \\ \gamma_s^\alpha(\tau) = \sum_{k \in \mathcal{M}_s} \frac{\phi_{k,s}}{\phi_s} S_{\chi_s, rt_k}^\alpha(\tau), & s \in \mathcal{V} \setminus \mathcal{V}_{Dir}, \end{cases} \quad (3.12)$$

that will be used in the accumulation terms. Using the Hybrid Upwinding approach, the VAG non-wetting phase Darcy fluxes are defined by

$$\mathcal{F}_{k,s}^{nw} = f_{k,s}^{nw,up} V_{k,s}^T + \underbrace{\frac{\sqrt{M_{k,s}^{nw,up}} \sqrt{M_{k,s}^{w,up}}}{M_k^T} \sum_{s' \in \mathcal{V}_k} \sqrt{M_{k,s'}^{nw}} \sqrt{M_{k,s'}^w} \mathbb{T}_k^{s,s'} \delta_{k,s'} p_{c,\mathcal{D}}}_{=F_{k,s}^d(p_{c,\mathcal{D}})} \quad (3.13)$$

and the VAG total velocity fluxes by

$$V_{k,s}^T = M_k^T \sum_{\alpha \in \{nw,w\}} \sum_{s' \in \mathcal{V}_k} \mathbb{T}_k^{s,s'} f_{rt_k}^\alpha(c_{k,s'}) \delta_{k,s'} p_{\mathcal{D}}^\alpha. \quad (3.14)$$

The VAG wetting phase Darcy fluxes are readily obtained by $\mathcal{F}_{k,s}^w = V_{k,s}^T - \mathcal{F}_{k,s}^{nw}$. In (3.13), the fractional flow is upwinded w.r.t the discrete total velocity

$$f_{k,s}^{nw,up} = \begin{cases} f_{rt_k}^{nw}(s_k^{nw}) & \text{if } V_{k,s}^T \geq 0, \\ f_{rt_k}^{nw}(s_{k,s}^{nw}) & \text{if } V_{k,s}^T < 0, \end{cases} \quad (3.15)$$

the mobilities in the capillary flux term are upwinded w.r.t. to $F_{k,s}^d(p_{c,\mathcal{D}})$ as follows

$$M_{k,s}^{nw,up} = \begin{cases} M_{rt_k}^{nw}(s_k^{nw}) & \text{if } F_{k,s}^d(p_{c,\mathcal{D}}) \geq 0, \\ M_{rt_k}^{nw}(s_{k,s}^{nw}) & \text{if } F_{k,s}^d(p_{c,\mathcal{D}}) < 0, \end{cases} \quad M_{k,s}^{w,up} = \begin{cases} M_{rt_k}^w(s_{k,s}^w) & \text{if } F_{k,s}^d(p_{c,\mathcal{D}}) \geq 0, \\ M_{rt_k}^w(s_k^w) & \text{if } F_{k,s}^d(p_{c,\mathcal{D}}) < 0, \end{cases} \quad (3.16)$$

and we set $M_{k,s}^\alpha = \frac{M_{\text{rt}_k}^\alpha(s_k^\alpha) + M_{\text{rt}_k}^\alpha(s_{k,s}^\alpha)}{2}$. In (3.14), the mean saturation $c_{k,s'}$ is defined as the unique solution of the nonlinear equation

$$f_{\text{rt}_k}^{\text{nw}}(c_{k,s'}^n)(G_{\text{rt}_k}^{\text{w}}(p_{c,k}^n) - G_{\text{rt}_k}^{\text{w}}(p_{c,s'}^n)) = f_{\text{rt}_k}^{\text{w}}(c_{k,s'}^n)(G_{\text{rt}_k}^{\text{nw}}(p_{c,k}^n) - G_{\text{rt}_k}^{\text{nw}}(p_{c,s'}^n)), \quad (3.17)$$

and the total mobility is defined by the following centered choice

$$M_k^T = M_{\text{rt}_k}(s_k^{\text{nw}}). \quad (3.18)$$

We will see in Section 4 that the definitions (3.13) and (3.14) of the VAG non-wetting and total velocity fluxes lead to the control of the global and mobility weighted capillary pressures and to the existence of a discrete solution. This was not the case of the previous HU-VAG scheme introduced in [16].

We consider a time discretization $t^0 = 0 < t^1 < \dots < t^{N-1} < t^N = t_f$ of the finite time-interval $[0, t_f]$ assumed to be uniform without any loss of generality such that $\delta t = \delta t^n = t^n - t^{n-1} = t_f/N$ for all $n \in \{1, \dots, N\}$. Given initial conditions $\tau_{\mathcal{D}}^0 \in [0, 1]^{\sharp(\mathcal{M} \cup \mathcal{V})}$, $p_{\mathcal{D}}^{\text{nw},0} \in \mathbb{R}^{\sharp(\mathcal{M} \cup \mathcal{V})}$, and Dirichlet boundary conditions such that for $s \in \mathcal{V}_{\text{Dir}}$, $\tau_{s,\text{Dir}} \in [0, 1]$ and $p_{s,\text{Dir}}^{\text{nw}} \in \mathbb{R}$. The implicit HU-VAG scheme looks for the solution $(p_{\mathcal{D}}^{\text{nw},n}, \tau_{\mathcal{D}}^n)$, $n = 1, \dots, N$ in $X_{\mathcal{D}}$ of the following system of balance equations and Dirichlet boundary conditions

$$\begin{cases} \frac{\phi_k}{\delta t^n} (\gamma_k^\alpha(\tau_k^n) - \gamma_k^\alpha(\tau_k^{n-1})) + \sum_{s \in \mathcal{V}_k} \mathcal{F}_{k,s}^{\alpha,n} = 0, & \forall k \in \mathcal{M}, \quad \forall \alpha \in \{\text{nw}, \text{w}\}, \\ \frac{\phi_s}{\delta t^n} (\gamma_s^\alpha(\tau_s^n) - \gamma_s^\alpha(\tau_s^{n-1})) - \sum_{k \in \mathcal{M}_s} \mathcal{F}_{k,s}^{\alpha,n} = 0, & \forall s \in \mathcal{V}/\mathcal{V}_{\text{Dir}}, \quad \forall \alpha \in \{\text{nw}, \text{w}\}, \\ p_s^{\text{nw},n} = p_{s,\text{Dir}}^{\text{nw}}, \quad \tau_s^n = \tau_{s,\text{Dir}}, & \forall s \in \mathcal{V}_{\text{Dir}}. \end{cases} \quad (3.19)$$

Summing the conservation equations over the phases provides an equivalent formulation of the system composed of a transport equation for the non-wetting phase and a divergence-free discrete equation for the total velocity as follows

$$\begin{cases} \frac{\phi_k}{\delta t^n} (\gamma_k^{\text{nw}}(\tau_k^n) - \gamma_k^{\text{nw}}(\tau_k^{n-1})) + \sum_{s \in \mathcal{V}_k} \mathcal{F}_{k,s}^{\text{nw},n} = 0, & \forall k \in \mathcal{M}, \\ \frac{\phi_s}{\delta t^n} (\gamma_s^{\text{nw}}(\tau_s^n) - \gamma_s^{\text{nw}}(\tau_s^{n-1})) - \sum_{k \in \mathcal{M}_s} \mathcal{F}_{k,s}^{\text{nw},n} = 0, & \forall s \in \mathcal{V}/\mathcal{V}_{\text{Dir}}, \\ \sum_{s \in \mathcal{V}_k} V_{k,s}^{T,n} = 0, & \forall k \in \mathcal{M}, \\ \sum_{k \in \mathcal{M}_s} -V_{k,s}^{T,n} = 0, & \forall s \in \mathcal{V}/\mathcal{V}_{\text{Dir}}, \\ p_s^{\text{nw},n} = p_{s,\text{Dir}}^{\text{nw}}, \quad \tau_s^n = \tau_{s,\text{Dir}}, & \forall s \in \mathcal{V}_{\text{Dir}}. \end{cases} \quad (3.20)$$

4. *A priori* ESTIMATES AND EXISTENCE RESULT

This section establishes *a priori* estimates for the solution of the numerical scheme (3.20). The proofs of Propositions 2 and 3 are deferred to Sections 4.1 and 4.2, respectively. Based on these *a priori* estimates, the existence of a discrete solution, as stated in Proposition 5, is then derived.

The first proposition states that any solution of (3.20) ensures that the saturations remain within the physical bounds of $[0, 1]$ or equivalently (due to (3.7) and (3.8)) that the primary unknown $\tau_{\mathcal{D}}^n$ is in $[0, 1]^{\sharp(\mathcal{M} \cup \mathcal{V})}$.

Proposition 2 (Maximum principle). *Let $\mathcal{F}_{k,s}^{\text{nw}}$ be the numerical fluxes given by (3.13). Then, for an initial condition $\tau_{\mathcal{D}}^0 \in [0, 1]^{\sharp(\mathcal{M} \cup \mathcal{V}/\mathcal{V}_{\text{Dir}})}$ and the given nodal data $\tau_{s,\text{Dir}} \in [0, 1]$ at Dirichlet boundary nodes, any solution $(p_{\mathcal{D}}^{\text{nw},n}, \tau_{\mathcal{D}}^n)$, $n = 1, \dots, N$, of the VAG-scheme satisfies the following maximum principle*

$$\tau_\nu^n \in [0, 1], \quad \text{for all } \nu \in \mathcal{M} \cup \mathcal{V}, \quad \forall n \in \{0, \dots, N\}. \quad (4.1)$$

The second proposition states that the global pressure and the mobility weighted capillary pressure satisfy energy estimates.

Proposition 3 (Energy estimates). *Let $(p_{\mathcal{D}}^{\text{nw}}, \tau_{\mathcal{D}})$ be a solution of the scheme (3.20), under the hypotheses $(A_0) - (A_5)$. Then, there exists a constant $C > 0$, depending on the mesh regularity parameters (3.2), (3.1), $\underline{\Lambda}$, $\overline{\Lambda}$, the initial data and Ω , but independent of the discretization parameters δt and $h_{\mathcal{T}}$ such that*

$$\sum_{n=1}^N \sum_{k \in \mathcal{M}} \delta t \sum_{s \in \mathcal{V}_k} F_{k,s}(\xi_{\text{rtk}}(p_{c,\mathcal{D}}^n)) (\xi_k^n - \xi_{k,s}^n) \leq C, \tag{4.2}$$

$$\sum_{n=1}^N \sum_{k \in \mathcal{M}} \delta t \sum_{s \in \mathcal{V}_k} F_{k,s}(p_{\mathcal{D}}^n) (p_k^n - p_{k,s}^n) \leq C. \tag{4.3}$$

Remark 4. In the above energy estimates, we assume for the sake of simplicity that the Dirichlet boundary conditions are homogeneous with $p_{s_{Dir}}^w = 0$ and $p_{s_{Dir}}^{\text{nw}} = 0$ for all $s \in \mathcal{V}_{Dir}$. Let us refer to [40] for a possible extension to non homogeneous Dirichlet boundary conditions.

The following Proposition states the existence of a solution to the numerical scheme (3.20). The proof is mainly based on the previous energy estimates. It follows the guidelines of [23].

Proposition 5 (Existence of a solution to (3.20)). *Under the hypotheses $(A_0) - (A_5)$ the scheme (3.20) admits at least a solution.*

We would like to emphasize that The HU-VAG scheme proposed in [16] suffers from some theoretical and numerical issues. First, it overestimates the approximation of the diffusion by taking a standard upwinding of the capillary fluxes. This leads to an additional numerical viscosity as exhibited in the first test of the numerical section. Second, there is no *a priori* estimation of energy type on the solution. Then, it does not allow to prove the existence of solutions for the coupled system. The new HU-VAG scheme is designed to circumvent these difficulties. It is stable in the sense that energy estimates are fulfilled. Moreover, one can prove the existence of a solution for both the saturation and the pressure. This is due to two key contributions. First, the upwinding thanks to the weighted capillary flux. Second, the particular choice of the saturation in the fractional flow functions of the total velocity.

4.1. Proof of the maximum principle

The property (4.1) holds true by assumption for $n = 0$ and for any Dirichlet node. We proceed by induction, assuming the result for any $0 \leq i \leq n - 1$ and we want to prove it at the time step n . We suppose that there exists $k \in \mathcal{M}$ such that

$$\tau_k^n = \min_{\nu \in \mathcal{M} \cup (\mathcal{V} \setminus \mathcal{V}_{Dir})} \tau_{\nu}^n < 0.$$

because of $\gamma_k^{\text{nw}}(\tau_k^n) < 0$, one has

$$\gamma_k^{\text{nw}}(\tau_k^{n-1}) = \gamma_k^{\text{nw}}(\tau_k^n) + \frac{\delta t}{\phi_k} \sum_{s \in \mathcal{V}_k} \mathcal{F}_{k,s}^{\text{nw},n} < \frac{\delta t}{\phi_k} \sum_{s \in \mathcal{V}_k} \mathcal{F}_{k,s}^{\text{nw},n}.$$

Taking a closer look at the non-wetting fluxes, owing to the degeneracy of the mobilities, one gets

$$\begin{aligned} \mathcal{F}_{k,s}^{\text{nw},n} &= f_{k,s}^{\text{nw},up,n} V_{k,s}^{T,n} + \frac{\sqrt{M_{k,s}^{\text{nw},up,n}} \sqrt{M_{k,s}^{\text{w},up,n}}}{M_k^{T,n}} F_{k,s}^d(p_{c,\mathcal{D}}^n) \\ &= f_{\text{rtk}}^{\text{nw}}(s_k^{\text{nw},n}) (V_{k,s}^{T,n})^+ - f_{\text{rtk}}^{\text{nw}}(s_{k,s}^{\text{nw},n}) (V_{k,s}^{T,n})^- \\ &\quad - \frac{\sqrt{M_{\text{rtk}}^{\text{nw}}(s_{k,s}^{\text{nw},n})} \sqrt{M_{\text{rtk}}^{\text{w}}(s_k^{\text{w},n})}}{M_k^{T,n}} (F_{k,s}^d(p_{c,\mathcal{D}}^n))^- + \frac{\sqrt{M_{\text{rtk}}^{\text{nw}}(s_k^{\text{nw},n})} \sqrt{M_{\text{rtk}}^{\text{w}}(s_{k,s}^{\text{w},n})}}{M_k^{T,n}} (F_{k,s}^d(p_{c,\mathcal{D}}^n))^+ \end{aligned}$$

$$= -f_{\text{rt}_k}^{\text{nw}}(s_{k,s}^{\text{nw},n}) \left(V_{k,s}^{T,n} \right)^- - \frac{\sqrt{M_{\text{rt}_k}^{\text{nw}}(s_{k,s}^{\text{nw},n})} \sqrt{M_{\text{rt}_k}^{\text{w}}(s_k^{\text{w},n})}}{M_k^{T,n}} \left(F_{k,s}^d(p_{c,\mathcal{D}}^n) \right)^- \leq 0.$$

It implies that $\gamma_k^{\text{nw}}(\tau_k^{n-1}) < 0$, which is absurd. One can proceed similarly if the minimum is reached for s in $\mathcal{V} \setminus \mathcal{V}_{\text{Dir}}$. Concerning the upper bound, if we assume it is violated for k in \mathcal{M} (the nodal case works similarly), one has

$$\tau_k^n = \max_{\nu \in \mathcal{M} \cup (\mathcal{V} \setminus \mathcal{V}_{\text{Dir}})} \tau_\nu^n > 1.$$

It follows that $\gamma_k^{\text{nw}}(\tau_k^n) > 1$, implying

$$\gamma_k^{\text{nw}}(\tau_k^{n-1}) = \gamma_k^{\text{nw}}(\tau_k^n) + \frac{\delta t}{\phi_k} \sum_{s \in \mathcal{V}_k} \mathcal{F}_{k,s}^{\text{nw},n} > 1 + \frac{\delta t}{\phi_k} \sum_{s \in \mathcal{V}_k} \mathcal{F}_{k,s}^{\text{nw},n}.$$

The VAG non-wetting phase fluxes are such that

$$\begin{aligned} \mathcal{F}_{k,s}^{\text{nw},n} &= f_{\text{rt}_k}^{\text{nw}}(s_k^{\text{nw},n}) \left(V_{k,s}^{T,n} \right)^+ - f_{\text{rt}_k}^{\text{nw}}(s_{k,s}^{\text{nw},n}) \left(V_{k,s}^{T,n} \right)^- + \frac{\sqrt{M_{\text{rt}_k}^{\text{nw}}(s_k^{\text{nw},n})} \sqrt{M_{\text{rt}_k}^{\text{w}}(s_{k,s}^{\text{w},n})}}{M_k^{T,n}} \left(F_{k,s}^d(p_{c,\mathcal{D}}^n) \right)^+ \\ &\geq \left(V_{k,s}^{T,n} \right)^+ - \left(V_{k,s}^{T,n} \right)^- = V_{k,s}^{T,n}. \end{aligned}$$

Then, using the discrete divergence-free equation for the total velocity (3.20), one gets

$$\gamma_k^{\text{nw}}(\tau_k^{n-1}) > \gamma_k^{\text{nw}}(\tau_k^n) + \frac{\delta t}{\phi_k} \sum_{s \in \mathcal{V}_k} \mathcal{F}_{k,s}^{\text{nw},n} > 1 + \frac{\delta t}{\phi_k} \sum_{s \in \mathcal{V}_k} V_{k,s}^{T,n} = 1.$$

It contradicts the induction hypothesis. Finally, the physical ranges hold true. The proof is complete.

4.2. Proof of the energy estimates

4.2.1. Preliminary lemmas

The following lemma establishes a key relationship between the discrete total velocity and the global pressure, serving as the discrete counterpart of the corresponding result in the continuous setting.

Lemma 6. *For all $k \in \mathcal{M}$ and $s \in \mathcal{V}_k$, the total velocity is linked to the global pressures by*

$$V_{k,s}^{T,n} = M_k^{T,n} \sum_{s' \in \mathcal{V}_k} \mathbb{T}_k^{s,s'} (p_k^n - p_{k,s'}^n). \tag{4.4}$$

Proof. Using (3.10) in the definition (3.14) of the total velocity we obtain

$$\begin{aligned} V_{k,s}^{T,n} &= M_k^{T,n} \sum_{\alpha \in \{\text{nw}, \text{w}\}} \sum_{s' \in \mathcal{V}_K} \mathbb{T}_k^{s,s'} f_{k,s'}^{\alpha,n} \delta_{k,s'} p_{\mathcal{D}}^{\alpha,n} \\ &= M_k^{T,n} \sum_{\alpha \in \{\text{nw}, \text{w}\}} \sum_{s' \in \mathcal{V}_K} \mathbb{T}_k^{s,s'} f_{k,s'}^{\alpha,n} \delta_{k,s'} p_{\mathcal{D}}^n \\ &\quad + M_k^{T,n} \sum_{s' \in \mathcal{V}_K} \mathbb{T}_k^{s,s'} \left(f_{k,s'}^{\text{nw},n} (G_{\text{rt}_k}^{\text{w}}(p_{c,k}^n) - G_{\text{rt}_k}^{\text{w}}(p_{c,s'}^n)) - f_{k,s'}^{\text{w},n} (G_{\text{rt}_k}^{\text{nw}}(p_{c,k}^n) - G_{\text{rt}_k}^{\text{nw}}(p_{c,s'}^n)) \right). \end{aligned} \tag{4.5}$$

This motivates the choice of $f_{k,s'}^{\alpha,n} = f_{\text{rt}_k}^{\alpha}(c_{k,s'}^n)$ with $c_{k,s'}$ defined by (3.17) such that the last term in the previous equality vanishes. Thus, one deduces from (4.5), (3.17), and $\sum_{\alpha \in \{\text{nw}, \text{w}\}} f_{k,s'}^{\alpha,n} = 1$, that

$$\begin{aligned} V_{k,s}^{T,n} &= M_k^{T,n} \sum_{\alpha \in \{\text{nw}, \text{w}\}} \sum_{s' \in \mathcal{V}_K} \mathbb{T}_k^{s,s'} f_{k,s'}^{\alpha,n} \delta_{k,s'} p_{\mathcal{D}}^{\alpha,n} \\ &= M_k^{T,n} \sum_{s' \in \mathcal{V}_K} \mathbb{T}_k^{s,s'} (p_k^n - p_{k,s'}^n). \end{aligned}$$

□

Remark 7. The equation (3.17) is equivalent to

$$f_{\text{rt}_k}^{\text{nw}}(c_{k,s'}^n)(p_{c,k}^n - p_{c,s'}^n) = (G_{\text{rt}_k}^{\text{nw}}(p_{c,k}^n) - G_{\text{rt}_k}^{\text{nw}}(p_{c,s'}^n)). \tag{4.6}$$

If $p_{c,k}^n = p_{c,s'}^n$, then we take $c_{k,s'}^n = s_{k,s'}^{\text{nw},n} = s_k^{\text{nw},n} \in [0, 1]$. Else, if $p_{c,k}^n \neq p_{c,s'}^n$, it means that $s_{k,s'}^{\text{nw},n} \neq s_k^{\text{nw},n}$ and that they are both in $[0, 1]$. Since $f_{\text{rt}_k}^{\text{nw}}(s)$ is strictly increasing on $(0, 1)$, and is equal to 0 for $s \leq 0$, and equal to 1 for $s \geq 1$, then, there exists a unique $c_{k,s'}^n$ in $(0, 1)$ satisfying (4.6).

Lemma 8. For all v, w in \mathbb{R} , the following estimate holds

$$\Pi_{\text{rt}_k}(v) - \Pi_{\text{rt}_k}(w) \leq v(S_{\chi_k, \text{rt}_k}^{\text{nw}}(v) - S_{\chi_k, \text{rt}_k}^{\text{nw}}(w)).$$

Setting $v = p_{c,k}^n$, and $w = p_{c,k}^{n-1}$, it results that for $n \in \{1, \dots, N\}$, $k \in \mathcal{M}$ and $s \in \mathcal{V}_k$ one has

$$\begin{aligned} \Pi_{\text{rt}_k}(p_{c,k}^n) - \Pi_{\text{rt}_k}(p_{c,k}^{n-1}) &\leq p_{c,k}^n \left(s_k^{\text{nw},n} - s_k^{\text{nw},n-1} \right), \\ \Pi_{\text{rt}_k}(p_{c,s}^n) - \Pi_{\text{rt}_k}(p_{c,s}^{n-1}) &\leq p_{c,s}^n \left(s_{k,s}^{\text{nw},n} - s_{k,s}^{\text{nw},n-1} \right). \end{aligned}$$

These estimates will be used to deal with the accumulation term in the energy estimates.

Proof. The proof follows the arguments of [12, 17]. □

In the two following Lemmas, we omit the time superscript for legibility.

Lemma 9. For each $k \in \mathcal{M}$, $s \in \mathcal{V}_k$, the following inequality holds true

$$\sqrt{M_{k,s}^{\text{nw},up}} \sqrt{M_{k,s}^{\text{w},up}} F_{k,s}^d(p_{c,\mathcal{D}})(p_{c,k} - p_{c,s}) \geq \sqrt{M_{k,s}^{\text{nw}}} \sqrt{M_{k,s}^{\text{w}}} F_{k,s}^d(p_{c,\mathcal{D}})(p_{c,k} - p_{c,s}).$$

Proof. This is done by disjunction of cases. Let $p_{c,\mathcal{D}} \in X_{\mathcal{D}}$ be given.

- We first consider the case $F_{k,s}^d(p_{c,\mathcal{D}}) \geq 0$ which implies that

$$\sqrt{M_{k,s}^{\text{nw},up}} \sqrt{M_{k,s}^{\text{w},up}} F_{k,s}^d(p_{c,\mathcal{D}})(p_{c,k} - p_{c,s}) = \sqrt{M_{\text{rt}_k}^{\text{nw}}(s_k^{\text{nw}})} \sqrt{M_{\text{rt}_k}^{\text{w}}(s_{k,s}^{\text{w}})} F_{k,s}^d(p_{c,\mathcal{D}})(p_{c,k} - p_{c,s}).$$

Two sub-cases are considered:

- If $s_k^{\text{nw}} \geq s_{k,s}^{\text{nw}}$, then $p_{c,k} \geq p_{c,s}$ (using the non-decreasing property of P_{c,χ_k} for any rt_k), and using the monotonicity of $M_{\text{rt}_k}^{\text{nw}}$ and $M_{\text{rt}_k}^{\text{w}}$, it follows that

$$\underbrace{\sqrt{M_{\text{rt}_k}^{\text{nw}}(s_k^{\text{nw}})}}_{\geq M_{k,s}^{\text{nw}}} \underbrace{\sqrt{M_{\text{rt}_k}^{\text{w}}(s_{k,s}^{\text{w}})}}_{\geq M_{k,s}^{\text{w}}} \underbrace{F_{k,s}^d(p_{c,\mathcal{D}})}_{\geq 0} \underbrace{(p_{c,k} - p_{c,s})}_{\geq 0} \geq \sqrt{M_{k,s}^{\text{nw}}} \sqrt{M_{k,s}^{\text{w}}} F_{k,s}^d(p_{c,\mathcal{D}})(p_{c,k} - p_{c,s}),$$

- else $s_k^{\text{nw}} < s_{k,s}^{\text{nw}}$, meaning that $p_{c,k} \leq p_{c,s}$, which lead to

$$\underbrace{\sqrt{M_{\text{rt}_k}^{\text{nw}}(s_k^{\text{nw}})}}_{\leq M_{k,s}^{\text{nw}}} \underbrace{\sqrt{M_{\text{rt}_k}^{\text{w}}(s_{k,s}^{\text{w}})}}_{\leq M_{k,s}^{\text{w}}} \underbrace{F_{k,s}^d(p_{c,\mathcal{D}})}_{\geq 0} \underbrace{(p_{c,k} - p_{c,s})}_{\leq 0} \geq \sqrt{M_{k,s}^{\text{nw}}} \sqrt{M_{k,s}^{\text{w}}} F_{k,s}^d(p_{c,\mathcal{D}})(p_{c,k} - p_{c,s}).$$

- Otherwise for $F_{k,s}^d(p_{c,\mathcal{D}}) < 0$, one gets

$$\sqrt{M_{k,s}^{\text{nw},up}} \sqrt{M_{k,s}^{\text{w},up}} F_{k,s}^d(p_{c,\mathcal{D}})(p_{c,k} - p_{c,s}) = \sqrt{M_{\text{rt}_k}^{\text{nw}}(s_{k,s}^{\text{nw}})} \sqrt{M_{\text{rt}_k}^{\text{w}}(s_k^{\text{w}})} F_{k,s}^d(p_{c,\mathcal{D}})(p_{c,k} - p_{c,s}).$$

As previously, two possible sub-cases are considered:

- Either we have $s_k^{nw} \geq s_{k,s}^{nw}$, which implies that $p_{c,k} \geq p_{c,s}$, then

$$\underbrace{\sqrt{M_{\text{rt}_k}^{nw}(s_{k,s}^{nw})}}_{\leq M_{k,s}^{nw}} \underbrace{\sqrt{M_{\text{rt}_k}^w(s_k^w)}}_{\leq M_{k,s}^w} \underbrace{F_{k,s}^d(p_{c,\mathcal{D}})}_{<0} \underbrace{(p_{c,k} - p_{c,s})}_{\geq 0} \geq \sqrt{M_{k,s}^{nw}} \sqrt{M_{k,s}^w} F_{k,s}^d(p_{c,\mathcal{D}})(p_{c,k} - p_{c,s}),$$

- or $s_k^{nw} < s_{k,s}^{nw}$ providing $p_{c,k} \leq p_{c,s}$ and

$$\underbrace{\sqrt{M_{\text{rt}_k}^{nw}(s_{k,s}^{nw})}}_{\geq M_{k,s}^{nw}} \underbrace{\sqrt{M_{\text{rt}_k}^w(s_k^w)}}_{\geq M_{k,s}^w} \underbrace{F_{k,s}^d(p_{c,\mathcal{D}})}_{<0} \underbrace{(p_{c,k} - p_{c,s})}_{\leq 0} \geq \sqrt{M_{k,s}^{nw}} \sqrt{M_{k,s}^w} F_{k,s}^d(p_{c,\mathcal{D}})(p_{c,k} - p_{c,s}).$$

The proof is completed. □

It results from Lemma 9 that for all $k \in \mathcal{M}$, we have

$$\sum_{s \in \mathcal{V}_k} \sqrt{M_{k,s}^{nw,up}} \sqrt{M_{k,s}^{w,up}} F_{k,s}^d(p_{c,\mathcal{D}})(p_{c,k} - p_{c,s}) \geq \sum_{s \in \mathcal{V}_k} \sqrt{M_{k,s}^{nw}} \sqrt{M_{k,s}^w} F_{k,s}^d(p_{c,\mathcal{D}})(p_{c,k} - p_{c,s}).$$

The following result shows an estimate between the discrete capillary and mobility weighted capillary pressures (3.11).

Lemma 10. *For each k in \mathcal{M} , there exists a constant $C_k > 0$ with $\frac{1}{4D} \leq C_k \leq \frac{1}{4}$ such that*

$$\sum_{s \in \mathcal{V}_k} \sqrt{M_{k,s}^{nw,up}} \sqrt{M_{k,s}^{w,up}} F_{k,s}^d(p_{c,\mathcal{D}})(p_{c,k} - p_{c,s}) \geq C_k \sum_{s \in \mathcal{V}_k} F_{k,s}(\xi_{\text{rt}_k}(p_{c,\mathcal{D}}))(\xi_k - \xi_{k,s}), \tag{4.7}$$

where D depends only on the mesh regularity parameters (3.2), (3.1) and on the lower and upper bounds $\underline{\Lambda}$ and $\bar{\Lambda}$ of the permeability tensor eigenvalues but not on the mesh size.

Proof. This proof is derived from the arguments provided in [20]. Since the mobilities are monotone functions, one has for any real interval $[a, b]$, $\max_{c \in [a,b]} \sqrt{M_{\text{rt}_k}^\alpha(c)} = \max(\sqrt{M_{\text{rt}_k}^\alpha(a)}, \sqrt{M_{\text{rt}_k}^\alpha(b)})$. Setting $\mathcal{I}_{k,s}^\alpha = [\min(s_k^\alpha, s_{k,s}^\alpha), \max(s_k^\alpha, s_{k,s}^\alpha)]$, one obtains

$$\sqrt{M_{k,s}^\alpha} \geq \frac{1}{\sqrt{2}} \max_{c \in \mathcal{I}_{k,s}^\alpha} \sqrt{M_{\text{rt}_k}^\alpha(c)}.$$

It follows that

$$|\xi_{k,s} - \xi_k| \leq \left(\max_{c \in \mathcal{I}_{k,s}^{nw}} \sqrt{M_{\text{rt}_k}^{nw}(c)} \right) \left(\max_{c' \in \mathcal{I}_{k,s}^w} \sqrt{M_{\text{rt}_k}^w(c')} \right) |p_{c,s} - p_{c,k}| \leq 2 \sqrt{M_{k,s}^{nw}} \sqrt{M_{k,s}^w} |p_{c,s} - p_{c,k}|.$$

For $k \in \mathcal{M}$, the diagonal square matrix $M_k(\tau_D)$ in $\mathbb{R}^{l_k \times l_k}$ is defined by

$$(M_k(\tau_D))_{s,s'} = \begin{cases} \sqrt{M_{k,s}^{nw}} \sqrt{M_{k,s}^w}, & \text{if } s = s', \\ 0, & \text{otherwise.} \end{cases}$$

Recalling the notation (3.5), we have the estimate

$$\begin{aligned} \|M_k(\tau_D) \delta_k p_{c,\mathcal{D}}\|_2^2 &= \sum_{s \in \mathcal{V}_k} M_{k,s}^{nw} M_{k,s}^w (p_{c,s} - p_{c,k})^2 \\ &\geq \frac{1}{4} \sum_{s \in \mathcal{V}_k} (\xi_{k,s} - \xi_k)^2 = \frac{1}{4} \|\delta_k \xi_{\text{rt}_k}(p_{c,\mathcal{D}})\|_2^2. \end{aligned}$$

Then, from the SPD property of the cell VAG transmissibility matrix A_k (3.4), we readily have that

$$v \cdot A_k v \geq w \cdot A_k w, \quad \forall v, w \in \mathbb{R}^{l_k} \quad \text{such that } |v|^2 \geq \text{Cond}_2(A_k)|w|^2,$$

from which we derive the estimate

$$\begin{aligned} M_k(\tau_{\mathcal{D}})\delta_k p_{c,\mathcal{D}} \cdot A_k M_k(\tau_{\mathcal{D}})\delta_k p_{c,\mathcal{D}} &\geq \frac{1}{4\text{Cond}_2(A_k)} \delta_k \xi_{\text{rt}_k}(p_{c,\mathcal{D}}) \cdot A_k \delta_k \xi_{\text{rt}_k}(p_{c,\mathcal{D}}) \\ &= \frac{1}{4\text{Cond}_2(A_k)} \int_k \Lambda(x) \nabla \pi_{\mathcal{T}} \xi_{\text{rt}_k}(p_{c,\mathcal{D}}) \cdot \nabla \pi_{\mathcal{T}} \xi_{\text{rt}_k}(p_{c,\mathcal{D}}) \, dx. \end{aligned}$$

Finally, the result is established by setting $C_k = \frac{1}{4\text{Cond}_2(A_k)}$. The proof is concluded by referring to Lemma 6.1 in the appendix of [20] stating that there exists a constant D depending only on the mesh regularity parameters (3.2), (3.1) and on the lower and upper bounds $\underline{\Lambda}, \bar{\Lambda}$ of the permeability tensor eigenvalues but not on the mesh size, such that $D > \text{Cond}_2(A_k) \geq 1$. \square

4.2.2. Proof of Proposition 3

For each degree of freedom $\nu \in \mathcal{M} \cup (\mathcal{V}/\mathcal{V}_{Dir})$, we multiply the non-wetting phase equation of the system (3.20) by the corresponding capillary pressure at the corresponding time-step n . Then, we sum it up over all degrees of freedom and time steps to get

$$\begin{aligned} \sum_{n=1}^N \delta t \left(\sum_{k \in \mathcal{M}} \left(\frac{\phi_k}{\delta t} (\gamma_k^{\text{nw}}(\tau_k^n) - \gamma_k^{\text{nw}}(\tau_k^{n-1})) + \sum_{s \in \mathcal{V}_k} \mathcal{F}_{k,s}^{\text{nw},n} \right) p_{c,k}^n \right. \\ \left. + \sum_{s \in \mathcal{V} \setminus \mathcal{V}_{Dir}} \left(\frac{\phi_s}{\delta t} (\gamma_s^{\text{nw}}(\tau_s^n) - \gamma_s^{\text{nw}}(\tau_s^{n-1})) - \sum_{k \in \mathcal{M}_s} \mathcal{F}_{k,s}^{\text{nw},n} \right) p_{c,s}^n \right) = 0. \end{aligned}$$

Using discrete integration by parts and taking into account the homogeneous Dirichlet boundary conditions according to Remark 4, we obtain

$$A_1 + A_2 + A_3 = 0,$$

with

$$\begin{aligned} A_1 &= \sum_{n=1}^N \delta t \left(\sum_{k \in \mathcal{M}} \frac{\phi_k}{\delta t} (\gamma_k^{\text{nw}}(\tau_k^n) - \gamma_k^{\text{nw}}(\tau_k^{n-1})) p_{c,k}^n + \sum_{s \in \mathcal{V} \setminus \mathcal{V}_{Dir}} \frac{\phi_s}{\delta t} (\gamma_s^{\text{nw}}(\tau_s^n) - \gamma_s^{\text{nw}}(\tau_s^{n-1})) p_{c,s}^n \right), \\ A_2 &= \sum_{n=1}^N \delta t \sum_{k \in \mathcal{M}} \sum_{s \in \mathcal{V}_k} f_{k,s}^{\text{nw},up,n} V_{k,s}^{T,n} (p_{c,k}^n - p_{c,s}^n), \\ A_3 &= \sum_{n=1}^N \delta t \sum_{k \in \mathcal{M}} \sum_{s \in \mathcal{V}_k} \frac{\sqrt{M_{k,s}^{\text{nw},up,n}} \sqrt{M_{k,s}^{\text{w},up,n}}}{M_k^{T,n}} F_{k,s}^d(p_{c,\mathcal{D}}) (p_{c,k}^n - p_{c,s}^n). \end{aligned}$$

The accumulation term A_1 is treated using Lemma 8 in a similar way as in [17], leading to the estimate

$$\begin{aligned}
 A_1 &\geq \left(\sum_{k \in \mathcal{M}} \phi_k (\Pi_{\text{rt}_k}(p_{c,k}^N) - \Pi_{\text{rt}_k}(p_{c,k}^0)) + \sum_{s \in \mathcal{V} \setminus \mathcal{V}_{D_{ir}}} \sum_{k \in \mathcal{M}} \phi_{k,s} (\Pi_{\text{rt}_k}(p_{c,s}^N) - \Pi_{\text{rt}_k}(p_{c,s}^0)) \right) \\
 &= \underbrace{\left(\sum_{k \in \mathcal{M}} \phi_k \Pi_{\text{rt}_k}(p_{c,k}^N) + \sum_{s \in \mathcal{V} \setminus \mathcal{V}_{D_{ir}}} \sum_{k \in \mathcal{M}} \phi_{k,s} \Pi_{\text{rt}_k}(p_{c,s}^N) \right)}_{A_{1,N}} \\
 &\quad - \underbrace{\left(\sum_{k \in \mathcal{M}} \phi_k \Pi_{\text{rt}_k}(p_{c,k}^0) + \sum_{s \in \mathcal{V} \setminus \mathcal{V}_{D_{ir}}} \sum_{k \in \mathcal{M}} \phi_{k,s} \Pi_{\text{rt}_k}(p_{c,s}^0) \right)}_{A_{1,0}}.
 \end{aligned} \tag{4.8}$$

Multiplying the discrete total velocity divergence-free equation in (3.20) by the corresponding wetting-phase pressure and summing over all degrees of freedom and time steps leads to

$$\sum_{n=1}^N \delta t \left(\sum_{k \in \mathcal{M}} \sum_{s \in \mathcal{V}_k} V_{k,s}^{T,n} p_k^{w,n} - \sum_{s \in \mathcal{V} \setminus \mathcal{V}_{D_{ir}}} \sum_{k \in \mathcal{M}_s} V_{k,s}^{T,n} p_s^{w,n} \right) = 0.$$

Injecting the global pressure definition (3.10) in the above equality, we obtain that

$$\sum_{n=1}^N \delta t \left(\sum_{k \in \mathcal{M}} \sum_{s \in \mathcal{V}_k} V_{k,s}^{T,n} (p_k^n - G_{\text{rt}_k}^{\text{nw}}(p_{c,k}^n)) - \sum_{s \in \mathcal{V} \setminus \mathcal{V}_{D_{ir}}} \sum_{k \in \mathcal{M}_s} V_{k,s}^{T,n} (p_{k,s}^n - G_{\text{rt}_k}^{\text{nw}}(p_{c,s}^n)) \right) = 0,$$

which also writes, taking into account the homogeneous Dirichlet boundary conditions

$$\underbrace{\sum_{n=1}^N \delta t \sum_{k \in \mathcal{M}} \sum_{s \in \mathcal{V}_k} V_{k,s}^{T,n} (p_k^n - p_{k,s}^n)}_{=B_1} = \underbrace{\sum_{n=1}^N \delta t \sum_{k \in \mathcal{M}} \sum_{s \in \mathcal{V}_k} V_{k,s}^{T,n} (G_{\text{rt}_k}^{\text{nw}}(p_{c,k}^n) - G_{\text{rt}_k}^{\text{nw}}(p_{c,s}^n))}_{=B_2}.$$

We deduce from Lemmas 6 and 1 that

$$\begin{aligned}
 B_1 &= \sum_{n=1}^N \delta t \sum_{k \in \mathcal{M}} M_k^{T,n} \sum_{s \in \mathcal{V}_k} \sum_{s' \in \mathcal{V}_k} \mathbb{T}_k^{s,s'} (p_k^n - p_{k,s}^n) (p_k^n - p_{k,s'}^n) \\
 &= \sum_{n=1}^N \delta t \sum_{k \in \mathcal{M}} M_k^{T,n} \int_k \Lambda(x) \nabla \pi_{\mathcal{T}} p_{\mathcal{D}}^n \cdot \nabla \pi_{\mathcal{T}} p_{\mathcal{D}}^n \, dx \\
 &\geq m_{\min} \sum_{n=1}^N \delta t \sum_{k \in \mathcal{M}} \sum_{s \in \mathcal{V}_k} F_{k,s}(p_{\mathcal{D}}^n) (p_k^n - p_{k,s}^n).
 \end{aligned} \tag{4.9}$$

Turning to the total velocity term A_2 , we first need to establish the estimate

$$f_{k,s}^{\text{nw},up,n} V_{k,s}^{T,n} (p_{c,k}^n - p_{c,s}^n) \geq f_{k,s}^{\text{nw},n} V_{k,s}^{T,n} (p_{c,k}^n - p_{c,s}^n), \tag{4.10}$$

which results from the non-decreasing property of $f_{\text{rt}_k}^{\text{nw}}$ for each rock-type rt_k . The proof proceeds by case disjunction as follows

- if $V_{k,s}^{T,n} \geq 0$, one has $f_{k,s}^{nw,up,n} = f_{rt_k}^{nw}(s_k^{nw,n})$, and two sub-cases must be investigated,
 - either $p_{c,k}^n - p_{c,s}^n \geq 0$ implying that $s_k^{nw,n} \geq c_{k,s}^n \geq s_{k,s}^{nw,n}$, then that $f_{k,s}^{nw,up,n} \geq f_{k,s}^{nw,n} \geq f_{rt_k}^{nw}(s_{k,s}^{nw,n})$;
 - or $p_{c,k}^n - p_{c,s}^n \leq 0$ implying that $s_k^{nw,n} \leq c_{k,s}^n \leq s_{k,s}^{nw,n}$, then that $f_{k,s}^{nw,up,n} \leq f_{k,s}^{nw,n} \leq f_{rt_k}^{nw}(s_{k,s}^{nw,n})$.
- else if $V_{k,s}^{T,n} < 0$ one has $f_{k,s}^{nw,up,n} = f_{rt_k}^{nw}(s_{k,s}^{nw,n})$ and we proceed in a similar way as the previous case.

This proves (4.10). Then, using (4.10) and the definition (4.6) of $c_{k,s}$, one infers

$$A_2 \geq \sum_{n=1}^N \delta t \sum_{k \in \mathcal{M}} \sum_{s \in \mathcal{V}_k} f_{k,s}^{nw,n} V_{k,s}^{T,n} (p_{c,k}^n - p_{c,s}^n) = \sum_{n=1}^N \delta t \sum_{k \in \mathcal{M}} \sum_{s \in \mathcal{V}_k} V_{k,s}^{T,n} (G_{rt_k}^{nw}(p_{c,k}^n) - G_{rt_k}^{nw}(p_{c,s}^n)) = B_2.$$

It follows from $B_2 = B_1$ and (4.9) that

$$A_2 \geq m_{\min} \sum_{n=1}^N \delta t \sum_{k \in \mathcal{M}} \sum_{s \in \mathcal{V}_k} F_{k,s}(p_{\mathcal{D}}^n)(p_k^n - p_{k,s}^n). \quad (4.11)$$

Turning to A_3 , Lemma 10 provides the estimate

$$\begin{aligned} A_3 &\geq \sum_{n=1}^N \delta t \sum_{k \in \mathcal{M}} \frac{C_k}{M_k^{T,n}} \sum_{s \in \mathcal{V}_k} F_{k,s}(\xi_{rt_k}(p_{c,\mathcal{D}}^n))(\xi_k^n - \xi_{k,s}^n) \\ &\geq \frac{1}{4DM_{\max}} \sum_{n=1}^N \delta t \sum_{k \in \mathcal{M}} \sum_{s \in \mathcal{V}_k} F_{k,s}(\xi_{rt_k}(p_{c,\mathcal{D}}^n))(\xi_k^n - \xi_{k,s}^n). \end{aligned} \quad (4.12)$$

Combining the estimates (4.8)–(4.11)–(4.12) with $A_1 + A_2 + A_3 = 0$ and using that the positivity of the capillary energy density Π_{rt_k} , we obtain that

$$\sum_{n=1}^N \delta t \left(\sum_{k \in \mathcal{M}} \sum_{s \in \mathcal{V}_k} F_{k,s}(\xi_{rt_k}(p_{c,\mathcal{D}}^n))(\xi_k^n - \xi_{k,s}^n) + F_{k,s}(p_{\mathcal{D}}^n)(p_k^n - p_{k,s}^n) \right) \leq \max \left(4DM_{\max}, \frac{1}{m_{\min}} \right) A_{1,0}.$$

which conclude the proof of Proposition 3.

5. NUMERICAL TESTS

In this section, the new Hybrid Upwinding VAG scheme (denoted by New HU in the following) is compared in terms of accuracy, efficiency and robustness to the previously introduced Hybrid Upwinding VAG scheme denoted by HU [15, 16] and to the VAG scheme combined with the classical Phase Potential Upwind strategy denoted by PPU and based on an upwind approximation of each phase mobility according to the sign of its Darcy velocity (see [30]).

In all test cases, the phase specific densities and dynamic viscosities are given by Table 1. All test cases include gravity effect with the gravitational acceleration set to $g = 10 \text{ m.s}^{-2}$, and consider a set $\mathcal{RT} = \{d, b\}$ of a drain d and barrier b rock-types. For each rock-type, the phase relative permeabilities are defined by $k_{r,rt}^\alpha(s^\alpha) = (s^\alpha)^{n_{rt}^\alpha}$, $\alpha \in \{nw, w\}$ and the capillary pressure is given by $P_{c,rt}(s^{nw}) = -b_{rt} \log(1 - s^{nw})$.

Following [14, 16], the parametrization (3.7) of the capillary pressure graphs is defined by $\tau = s^{nw}$ for all cells and for all nodes belonging to a single rock-type subdomain, and by

$$S_{\{b,d\},d}^{nw}(\tau) = \begin{cases} \tau, & \tau \in [0, \tau_1), \\ 1 - (\tau_1 + (1 - \tau_1)^{\frac{b_d}{b_b}} - \tau)^{\frac{b_b}{b_d}}, & \tau \in [\tau_1, \tau_2), \end{cases} \quad (5.1)$$

$$S_{\{b,d\},b}^{nw}(\tau) = \begin{cases} 1 - (1 - \tau)^{\frac{b_d}{b_b}}, & \tau \in [0, \tau_1), \\ \tau - \tau_1 + 1 - (1 - \tau_1)^{\frac{b_d}{b_b}}, & \tau \in [\tau_1, \tau_2), \end{cases} \quad (5.2)$$

TABLE 1. Phases thermodynamical properties.

Quantity	Notation	Dimension	Value
Non-wetting phase density	ρ_{nw}	[Kg/m ³]	700
Wetting phase density	ρ_w	[Kg/m ³]	1000
Non-wetting phase dynamic viscosity	μ_{nw}	[Pa.s]	0.005
Wetting phase dynamic viscosity	μ_w	[Pa.s]	0.001

$$P_{c,\{b,d\}}(\tau) = \begin{cases} -b_d \ln(1 - \tau), & \tau \in [0, \tau_1), \\ -b_b \ln(\tau_1 + (1 - \tau_1)^{\frac{b_d}{b_b}} - \tau), & \tau \in [\tau_1, \tau_2), \end{cases} \quad (5.3)$$

for all nodes belonging to both rock-type subdomains, with $\tau_1 = 1 - (\frac{b_d}{b_b})^{\frac{b_b}{b_b - b_d}}$ and $\tau_2 = \tau_1 + (1 - \tau_1)^{\frac{b_d}{b_b}}$ (see Fig. 1).

In the following simulations, the time stepping is defined by $\Delta t^1 = \Delta t_{init}$, and for all $n \geq 1$, by

$$\Delta t^{n+1} = \min(\Delta t_{\max}, 1.2\Delta t^n)$$

in case of a successful time step Δt^n , and $\Delta t^{n+1} = \frac{\Delta t^n}{2}$, in case of non convergence of the Newton algorithm in 25 iterations. At each time step, the nonlinear system is solved using a Newton algorithm. The cell unknowns are eliminated without any fill-in before solving the linear system using a GMRES iterative algorithm preconditioned by the CPR-AMG preconditioner [36,42]. To obtain a more robust convergence of the nonlinear solver, a damping of the Newton step forces a maximum variation of 1 of the τ discrete unknown. This strategy is applied for all test cases and all schemes. Let us denote by $(R_\nu(p_{\mathcal{D}}^{nw}, \tau_{\mathcal{D}}))_{\nu \in \mathcal{M}_{UV}}$ the residual of equations (3.19) with $R_\nu = (R_\nu^1, R_\nu^2) \in \mathbb{R}^2$, and its norm

$$\|R\|_1 = \sum_{\nu \in \mathcal{M}_{UV}} |R_\nu^1| + |R_\nu^2|.$$

Let us also denote by $(dp_{\mathcal{D}}^{nw}, d\tau_{\mathcal{D}})$ the solution of the Newton Jacobian system and define $\|dp_{\mathcal{D}}^{nw}\|_\infty = \max_{\nu \in \mathcal{M}_{UV}} |dp_\nu^{nw}|$, $\|d\tau_{\mathcal{D}}\|_\infty = \max_{\nu \in \mathcal{M}_{UV}} |d\tau_\nu|$. The Newton solver is convergent if the relative residual $\frac{\|R\|_1}{\|R^{(0)}\|_1}$ is lower than 10^{-5} with $R^{(0)}$ the initial residual, or if the weighted maximum norm of the Newton increment $\|d\tau_{\mathcal{D}}\|_\infty + 10^{-5}\|dp_{\mathcal{D}}^{nw}\|_\infty$ is lower than 10^{-4} . The GMRES stopping criterion on the relative residual is fixed to 10^{-6} .

We denote by $N_{\Delta t}$ the number of successful time steps, by N_{Chop} the number of time step chops, by N_{Newton} the average number of Newton iterations per successful time step, and by N_{GMRES} the average number of GMRES iterations per Newton iteration. Finally, CPU (s) stands for the CPU time in seconds.

5.1. Oil migration in a 1D basin with capillary barrier

To compare the accuracy of the three VAG schemes, we first consider a slightly modified version (regarding capillary pressures) of the 1D basin test case introduced in [16]. The basin domain is defined by $\Omega = (0, L_x) \times (0, L_y) \times (0, L_z)$ with $L_x = L_y = 10$ m and $L_z = 800$ m including a drain rock-type on $\Omega_d = (0, L_x) \times (0, L_y) \times (0, \frac{L_z}{2})$ and a barrier rock-type on $\Omega_b = \Omega \setminus \overline{\Omega}_d$. The dynamic petrophysical properties are defined by $n_d^\alpha = n_b^\alpha = 2$, $b_d = 10^4$ Pa, $b_b = 6 \cdot 10^5$ Pa. To enhance the capillary barrier effect, the porosity and absolute permeability are taken homogeneous with $\phi = 0.2$ and $\Lambda = 10^{-13}$ m². The basin is initially saturated by the wetting phase and the non-wetting phase migrates by gravity during the 150 years of simulation from the bottom boundary at which the fixed saturation $s^{nw} = 0.5$ is prescribed. All meshes are uniform with only one cell in the x and y directions and capture the interface between both rock-type subdomains. Let us refer to [16] for a more detailed description of the test case. The time stepping is defined by $\Delta t_{init} = 1$ day and $\Delta t_{\max} = 360$ days.

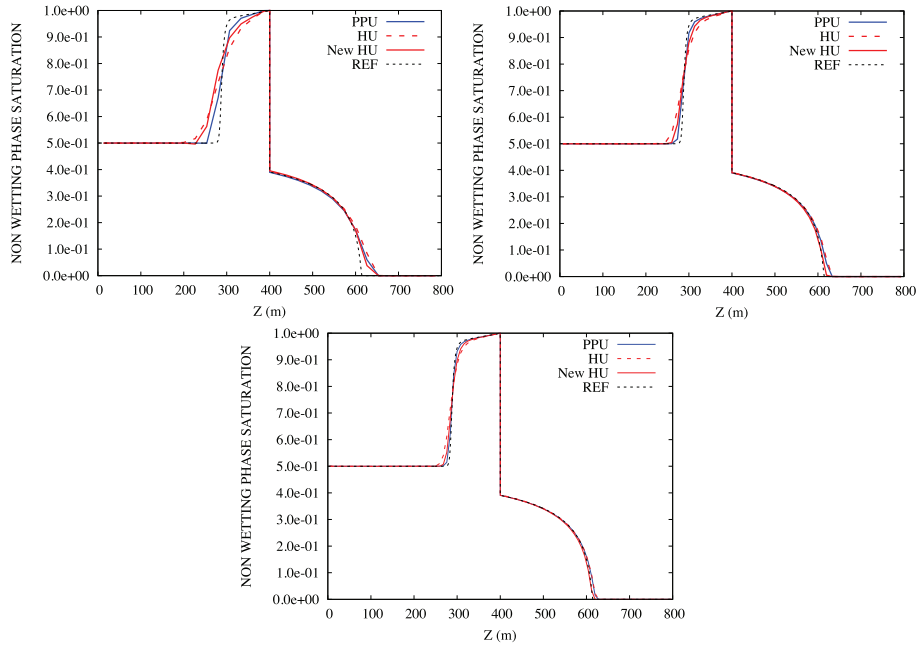


FIGURE 2. Non-wetting phase saturations as a function of z at final time $t_f = 150$ years, obtained for the PPU, HU and New-HU-VAG schemes on the 30 (*left top*), 60 (*right top*), and 100 cells (*bottom*) meshes. The reference solution is obtained with the PPU VAG scheme on a 800 cells mesh.

TABLE 2. For the three VAG schemes on the 100 cells mesh: number of successful time steps $N_{\Delta t}$, number of the time step chops N_{chop} , total number of Newton iterations, average number of GMRES iterations per Newton step N_{GMRes} .

Scheme	$N_{\Delta t}$	N_{chop}	N_{Newton}	N_{GMRes}
PPU	202	0	868	6.3
HU	202	0	727	6.0
New HU	202	0	730	6.0

Hybrid Upwinding schemes are known to be more diffusive than the PPU scheme since they combine the diffusion of the total velocity, capillary and gravity terms. This can be checked in Figure 2 showing that the PPU scheme exhibits the smaller diffusion of the left front before the barrier. We also notice that the New HU-VAG scheme is less diffusive than the HU-VAG scheme, with a left front basically in between the PPU and HU solutions. This is because the new HU-VAG method provides a more accurate and stable approximation of the continuous capillary term by incorporating square roots of the mobilities. In contrast, the standard HU-VAG approach uses a simpler upwinding scheme for the mobilities in the diffusive fluxes, which leads to a less accurate representation translated into numerical diffusion. On the other hand, all schemes capture in an excellent way the saturation jump at the interface between both rock-types. Table 2 exhibits the gain in terms of nonlinear convergence obtained with both HU VAG schemes compared to the PPU VAG scheme, even for this rather simple 1D test case. This is known to result from the better smoothness properties of the HU fluxes compared with the PPU fluxes [32, 34].

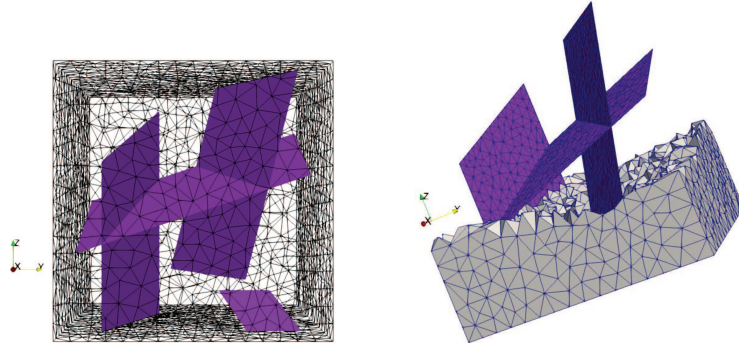


FIGURE 3. Geometrical configuration of the matrix domain and the fracture network meshed with 47 670 tetrahedra and 1670 fracture faces.

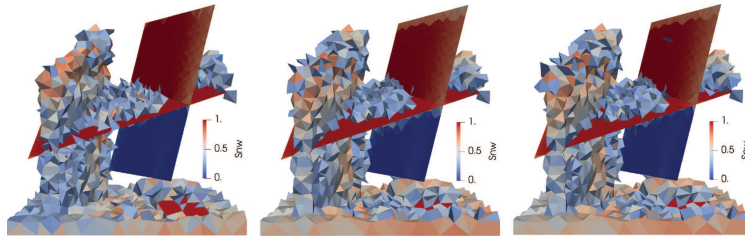


FIGURE 4. From *left to right*, non-wetting phase saturation along the fracture network and in the matrix (above the threshold 0.25) for the PPU, HU and New HU-VAG schemes.

5.2. Small 3D Discrete Fracture Matrix model (DFM)

We consider the test case introduced in [15] which simulates the oil migration in a fractured reservoir $\Omega = (0, 100 \text{ m})^3$. The fracture network is modeled as a set of co-dimension one planar fractures Ω_d acting as a drain with aperture $d_f = 10^{-2} \text{ m}$, porosity $\phi_d = 0.4$, and tangential permeability $\Lambda_d = 10^{-10} \text{ m}^2$. The surrounding matrix domain $\Omega_b = \Omega \setminus \Omega_d$ is homogeneous with porosity $\phi_b = 0.2$, and isotropic permeability $\Lambda_b = 10^{-16} \text{ m}^2$ highly contrasted with respect to the fracture network. The dynamic petrophysical properties are given by the parameters $n_b^\alpha = 2$, $n_d^\alpha = 1.2$, $b_b = 10^4 \text{ Pa}$, $b_d = 10^3 \text{ Pa}$. The domain is discretized using a tetrahedral mesh conforming to the fracture network and consisting of 47 670 cells and 1670 fracture faces (see Fig. 3). Let us refer to [13, 14] for the description of the DFM two-phase flow model based on the continuous pressure assumption at matrix fracture interfaces, and for the extension of the VAG discretization to such model.

The non-wetting phase is injected from the bottom boundary in the reservoir initially saturated with the wetting phase. Dirichlet boundary conditions are imposed at the top boundary with a wetting phase pressure of 1 MPa and $s_b^w = 1$, as well as at the bottom boundary with $p^w = 4.10^6 \text{ Pa}$ and $s_b^{nw} = 0.9$. The lateral boundaries are impervious. The final simulation time is fixed to $t_f = 3600$ days, and the time stepping is defined by $\Delta t_{init} = 0.01$ day and $\Delta t_{max} = 100$ days.

We display in Figures 4–6 and in Table 3 the results obtained for the PPU, HU, and New HU-VAG discretizations. Both HU schemes provide basically the same solutions while small differences can be observed between the HU and PPU schemes. These differences have been checked in [15] to partially result from the centered approximation of the total mobility term for the HU schemes especially at the input boundary compared with the upwind PPU approximation.

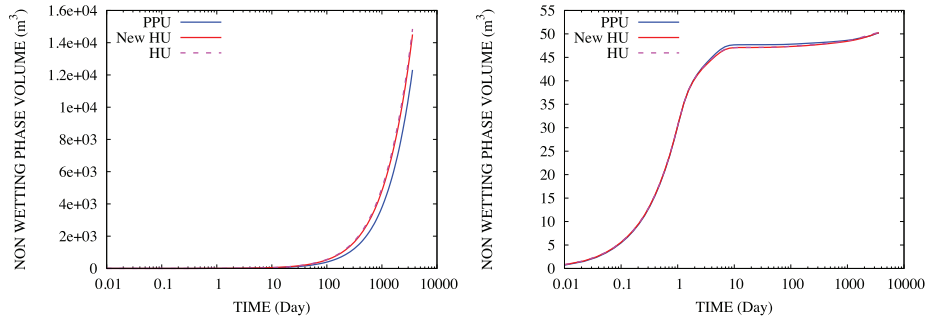


FIGURE 5. Non wetting-phase volume as a function of time in the matrix (*left*) and in the fracture network (*right*) for the three VAG schemes (small 3D DFM test case).

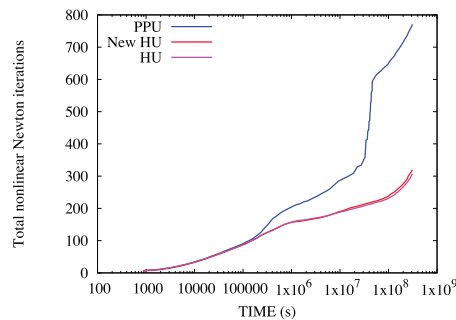


FIGURE 6. Accumulated number of Newton iterations as a function of time for the three VAG schemes (small 3D DFM test case).

TABLE 3. Number of successful time steps $N_{\Delta t}$, number of the time step chops N_{chop} , average number of Newton iterations per time step N_{Newton} , average number of GMRES iterations per Newton step N_{GMRES} and CPU time for the three VAG schemes (small 3D DFM test case).

Scheme	$N_{\Delta t}$	N_{chop}	N_{Newton}	N_{GMRES}	CPU (s)
PPU	106	8	6.7	14.9	341
HU	82	0	3.8	13.8	142
New HU	82	0	3.9	13.6	163

The nonlinear convergence exhibited in Figure 6 and Table 3 shows, as in the 1D basin test case, a more robust and efficient behavior of both HU-VAG schemes compared with the PPU VAG scheme. It is remarkable that this property, resulting from the better smoothness properties of the HU fluxes, extends to the New HU scheme with only a slight overcost due to the additional complexity of the new HU scheme fluxes. To challenge the robustness of the schemes, we have tested an initial time step of 10 days which basically corresponds to fill the fractures in a single time step (see Fig. 5). The number of Newton iterations obtained for this single time step is 31 for the HU scheme, 41 for the new HU scheme, while the PPU scheme only converges after 10 time step chops down to roughly 10^{-2} day.



FIGURE 7. Large DFM model meshed with 495 233 tetrahedra and 66 908 fracture faces.

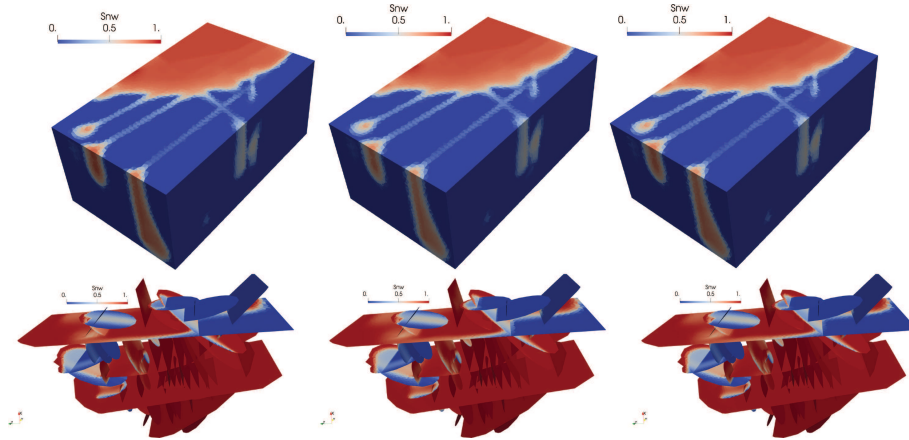


FIGURE 8. Non-wetting phase saturation in the matrix (*top*) and in the fracture network (*bottom*) at final simulation time obtained for the PPU (*left*), HU (*middle*) and New HU (*right*) VAG schemes.

5.3. Large 3D Discrete Fracture Matrix model (DFM)

To further assess the robustness of the New HU-VAG scheme, we consider the test case introduced in [16] based on the large DFM provided by the Benchmark [8] and exhibited in Figure 7. The domain is defined by $\Omega = (0, 85) \times (0, 60) \times (0, 140)$ m and includes a co-dimension one fracture network with 52 fractures of constant aperture $d_f = 10^{-2}$ m, tangential permeability $\Lambda_d = 10^{-11}$ m² and porosity $\phi_d = 0.2$. The matrix is homogeneous with isotropic permeability $\Lambda_b = 10^{-14}$ m² and porosity $\phi_b = 0.4$. The dynamic petrophysical properties are defined by the parameters $n_b^\alpha = 2$, $n_d^\alpha = 1.2$, $b_b = 10^4$ Pa, $b_d = 10^3$ Pa.

The reservoir is initially saturated with the wetting phase. Dirichlet boundary conditions are imposed at the output boundary $\{0, 85\} \times (0, 20) \times (110, 140)$ with a wetting phase pressure of $p^w = 2 \cdot 10^6 - \rho_w g z$ Pa and $s_b^w = 1$, as well as at the input boundary $\{0\} \times (40, 60) \times (0, 30) \cup (0, 30) \times (40, 85) \times \{0\}$ with $s_b^{nw} = 0.9$ and $p^w = 4 \cdot 10^6 - \rho_w g z$ Pa. The remaining boundaries are impervious and the final simulation time is fixed to $t_f = 3600$ days. The time stepping is defined by $\Delta t_{init} = 0.1$ day, and $\Delta t_{max} = 100$ days.

Figure 8 show that the non-wetting saturations obtained at final time by the PPU and both HU-VAG schemes are almost the same. Small differences can be noticed on the top right part of the fracture network in Figure 8 showing again that the solution of the New HU scheme is somewhat in between the solutions of the original HU and PPU schemes.

Table 4 and Figure 9 compare the numerical efficiency of the three VAG schemes. Compared with the PPU scheme, the nonlinear convergence of the HU schemes is more robust (no time step failure against 3 time step chops for PPU) and more efficient (average of 4 to 4.5 Newton iterations for the HU schemes against 6.4 for

TABLE 4. Number of successful time steps $N_{\Delta t}$, number of the time step chops N_{chop} , average number of Newton iterations per time step N_{Newton} , average number of GMRES iterations per Newton step N_{GMRes} and CPU time for the three VAG schemes (large 3D DFM test case).

Scheme	$N_{\Delta t}$	N_{chop}	N_{Newton}	N_{GMRes}	CPU (s)
PPU	77	3	6.4	28	4570
HU	69	0	4.1	33	2820
New HU	69	0	4.5	32	3230

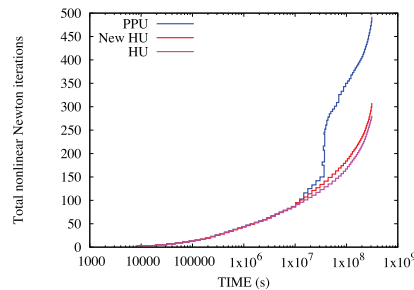


FIGURE 9. Accumulated number of Newton iterations as a function of time for the three VAG schemes (large 3D DFM test case).

PPU) resulting in an overall gain in CPU time of a factor roughly 1.5 in favor of both HU-VAG schemes. The New HU-VAG scheme is slightly more costly than the original HU scheme but remains much more robust and efficient than the PPU scheme.

6. CONCLUSION

We developed a new Hybrid Upwinding VAG scheme for the discretization of incompressible two-phase Darcy flow in heterogeneous porous media. Two main challenges are encountered in the numerical analysis of these types of systems. First, there is a strong coupling of mass conservation laws, especially in the presence of discontinuous capillary forces. Second, the Multi-Point character of the VAG discretization method on general polyhedral meshes makes it difficult to obtain stability results. Based on the total velocity formulation of the diphasic model as well as on a parameterization of the capillary pressure graph, we introduce a particular approximation of the fluxes in order to derive the main *a priori* estimates. For this purpose, the capillary term is approximated thanks to the positive upwinding scheme with particular choices of the mobilities. Additionally, some nonlinear equalities are imposed to link the total velocity to the global pressure function. These *a priori* estimates are the cornerstone to prove the existence of a numerical solution. Numerical experiments show that this new HU-VAG scheme is still much more robust than the standard PPU scheme and provides a gain in accuracy compared with the previously introduced HU-VAG scheme [16].

REFERENCES

- [1] E. Ahmed, C. Japhet and M. Kern, Space–time domain decomposition for two-phase flow between different rock types. *Comput. Methods Appl. Mech. Eng.* **371** (2020) 113294.
- [2] S.N. Antontsev, A. Kazhikov and V.N. Monakhov, *Boundary Value Problems in Mechanics of Nonhomogeneous Fluids*. Elsevier (1989).
- [3] A. Armandine Les Landes, L. Beaudé, D. Castanon Quiroz, L. Jeannin, S. Lopez, F. Smal, T. Guillon and R. Masson, Geothermal modeling in complex geological systems with compass. *Comput. Geosci.* **194** (2025) 105752.

- [4] K. Aziz, Petroleum reservoir simulation. *Appl. Sci. Publ.* (1979) 476.
- [5] P. Bastian, *Numerical computation of multiphase flows in porous media*. Ph.D. thesis, Habilitationsschrift Universität Kiel (1999).
- [6] P. Bastian, A fully-coupled discontinuous galerkin method for two-phase flow in porous media with discontinuous capillary pressure. *Comput. Geosci.* **18** (2014) 779–796.
- [7] J. Bear, *Dynamics of Fluids in Porous Media*. Courier Corporation (2013).
- [8] I. Berre, W.M. Boon, B. Flemisch, A. Fumagalli, D. Gläser, E. Keilegavlen, A. Scotti, I. Stefansson, A. Tatomir, K. Brenner, S. Burbulla, P. Devloo, O. Duran, M. Favino, J. Hennicker, I.-H. Lee, K. Lipnikov, R. Masson, K. Mosthaf, M.G.C. Nestola, C.-F. Ni, K. Nikitin, P. Schädle, D. Svyatskiy, R. Yanbarisov and P. Zulian, Verification benchmarks for single-phase flow in three-dimensional fractured porous media. *Advan. Water Resour.* **147** (2021) 103759.
- [9] M. Bertsch, R.D. Passo and C.J. Van Duijn, Analysis of oil trapping in porous media flow. *SIAM J. Math. Anal.* **35** (2003) 245–267.
- [10] Y. Brenier and J. Jaffré, Upstream differencing for multiphase flow in reservoir simulation. *SIAM J. Numer. Anal.* **28** (1991) 685–696.
- [11] K. Brenner and R. Masson, Convergence of a vertex centred discretization of two-phase Darcy flows on general meshes. *Int. J. Finite Vol.* **10** (2013) 1–37.
- [12] K. Brenner, C. Cancès and D. Hilhorst, Finite volume approximation for an immiscible two-phase flow in porous media with discontinuous capillary pressure. *Comput. Geosci.* **17** (2013) 573–597.
- [13] K. Brenner, M. Groza, C. Guichard and R. Masson, Vertex approximate gradient scheme for hybrid dimensional two-phase Darcy flows in fractured porous media. *ESAIM: Math. Modell. Numer. Anal.* **49** (2015) 303–330.
- [14] K. Brenner, M. Groza, L. Jeannin, R. Masson and J. Pellerin, Immiscible two-phase Darcy flow model accounting for vanishing and discontinuous capillary pressures: application to the flow in fractured porous media. *Comput. Geosci.* **21** (2017) 1075–1094.
- [15] K. Brenner, R. Masson and E.H. Quenjel, A robust VAG scheme for a two-phase flow problem in heterogeneous porous media, in *Finite Volumes for Complex Applications IX – Methods, Theoretical Aspects, Examples*, edited by R. Klöforn, E. Keilegavlen, F.A. Radu and J. Fuhrmann. Springer International Publishing, Cham (2020) 565–573.
- [16] K. Brenner, R. Masson and E.-H. Quenjel, Vertex approximate gradient discretization preserving positivity for two-phase darcy flows in heterogeneous porous media. *J. Comput. Phys.* **409** (2020) 109357.
- [17] K. Brenner, R. Masson, E.-H. Quenjel and J. Droniou, Total velocity-based finite volume discretization of two-phase Darcy flow in highly heterogeneous media with discontinuous capillary pressure. *IMA J. Numer. Anal.* **42** (2021) 1231–1272.
- [18] F. Buzzi, M. Lenzinger and B. Schweizer, Interface conditions for degenerate two-phase flow equations in one space dimension. *Analysis* **29** (2009) 299–316.
- [19] C. Cancès, Finite volume scheme for two-phase flows in heterogeneous porous media involving capillary pressure discontinuities. *ESAIM: Math. Modell. Numer. Anal.* **43** (2009) 973–1001.
- [20] C. Cancès and C. Guichard, Numerical analysis of a robust free energy diminishing finite volume scheme for parabolic equations with gradient structure. *Found. Comput. Math.* **17** (2017) 1525–1584.
- [21] C. Cancès and M. Pierre, An existence result for multidimensional immiscible two-phase flows with discontinuous capillary pressure field. *SIAM J. Math. Anal.* **44** (2012) 966–992.
- [22] G. Chavent and J. Jaffré, *Mathematical Models and Finite Elements for Reservoir Simulation: Single Phase, Multiphase and Multicomponent Flows Through Porous Media*. Elsevier (1986).
- [23] T. Crozon, Existence of solutions to numerical schemes using regularization: application to two-phase flow in porous media schemes. Preprint [arXiv:2411.09285](https://arxiv.org/abs/2411.09285) (2024).
- [24] G. Enchéry, *Modèles et schémas numériques pour la simulation de génèse de bassins sédimentaires*. Ph.D. thesis, Université de Marne-la-Vallée (2004).
- [25] G. Enchéry, R. Masson, S. Wolf and R. Eymard, Mathematical and numerical study of an industrial scheme for two-phase flows in porous media under gravity. *Comput. Methods Appl. Math.* **2** (2002) 325–353.
- [26] G. Enchéry, R. Eymard and A. Michel, Numerical approximation of a two-phase flow problem in a porous medium with discontinuous capillary forces. *SIAM J. Numer. Anal.* **43** (2006) 2402–2422.
- [27] A. Ern, I. Mozolevski and L. Schuh, Discontinuous Galerkin approximation of two-phase flows in heterogeneous porous media with discontinuous capillary pressures. *Comput. Methods Appl. Mech. Eng.* **199** (2010) 1491–1501.
- [28] R. Eymard, T. Gallouët and R. Herbin, Discretization of heterogeneous and anisotropic diffusion problems on general nonconforming meshes sushi: a scheme using stabilization and hybrid interfaces. *IMA J. Numer. Anal.* **30** (2010) 1009–1043.

- [29] R. Eymard, C. Guichard and R. Herbin, Small-stencil 3D schemes for diffusive flows in porous media. *ESAIM: Math. Modell. Numer. Anal.-Modél. Math. Anal. Numér.* **46** (2012) 265–290.
- [30] R. Eymard, C. Guichard, R. Herbin and R. Masson, Vertex-centred discretization of multiphase compositional Darcy flows on general meshes. *Comput. Geosci.* **16** (2012) 987–1005.
- [31] R. Eymard, C. Guichard, R. Herbin and R. Masson, Gradient schemes for two-phase flow in heterogeneous porous media and Richards equation. *ZAMM-J. Appl. Math. Mech./Z. Ang. Math. Mech.* **94** (2014) 560–585.
- [32] F.P. Hamon and B.T. Mallison, Fully implicit multidimensional hybrid upwind scheme for coupled flow and transport. *Comput. Methods Appl. Mech. Eng.* **358** (2020) 112606.
- [33] F.P. Hamon and H.A. Tchelepi, Analysis of hybrid upwinding for fully-implicit simulation of three-phase flow with gravity. *SIAM J. Numer. Anal.* **54** (2016) 1682–1712.
- [34] F.P. Hamon, B.T. Mallison and H.A. Tchelepi, Implicit hybrid upwinding for two-phase flow in heterogeneous porous media with buoyancy and capillarity. *Comput. Methods Appl. Mech. Eng.* **331** (2018) 701–727.
- [35] H. Hoteit and A. Firoozabadi, An efficient numerical model for incompressible two-phase flow in fractured media. *Adv. Water Resour.* **31** (2008) 891–905.
- [36] S. Lacroix, Y.V. Vassilevski and M.F. Wheeler, Decoupling preconditioners in the implicit parallel accurate reservoir simulator (IPARS). *Numer. Linear Algebra Appl.* **8** (2001) 537–549.
- [37] J.E. Montegudo and A. Firoozabadi, Control-volume model for simulation of water injection in fractured media: incorporating matrix heterogeneity and reservoir wettability effects. *SPE J.* **12** (2007) 355–366.
- [38] D.W. Peaceman, *Fundamentals of Numerical Reservoir Simulation*. Developments in Petroleum Science. Elsevier Scientific Publishing Company (1977).
- [39] E.-H. Quenjel, Enhanced positive vertex-centered finite volume scheme for anisotropic convection-diffusion equations. *ESAIM: Math. Modell. Numer. Anal.* **54** (2020) 591–618.
- [40] E.-H. Quenjel, P. Perré and I. Turner, A 3D face interpolated discretisation method for simulating anisotropic diffusive processes on meshes coming from wood morphology. *Appl. Numer. Math.* **192** (2023) 280–296.
- [41] V. Reichenberger, H. Jakobs, P. Bastian and R. Helmig, A mixed-dimensional finite volume method for two-phase flow in fractured porous media. *Adv. Water Resour.* **29** (2006) 1020–1036.
- [42] R. Scheichl, R. Masson and J. Wendebourg, Decoupling and block preconditioning for sedimentary basin simulations. *Comput. Geosci.* **7** (2003) 295–318.
- [43] C. Van Duijn, J. Molenaar and M. De Neef, The effect of capillary forces on immiscible two-phase flow in heterogeneous porous media. *Transp. Porous Med.* **21** (1995) 71–93.



Please help to maintain this journal in open access!

This journal is currently published in open access under the Subscribe to Open model (S2O). We are thankful to our subscribers and supporters for making it possible to publish this journal in open access in the current year, free of charge for authors and readers.

Check with your library that it subscribes to the journal, or consider making a personal donation to the S2O programme by contacting subscribers@edpsciences.org.

More information, including a list of supporters and financial transparency reports, is available at <https://edpsciences.org/en/subscribe-to-open-s2o>.